

1 DR5 disulfide bonding as a sensor and effector of protein folding stress

2
3 Mary E. Law^{1*}, Zaafir M. Dulloo^{2*}, Samantha R. Eggleston², Gregory P. Takacs¹, Grace M. Alexandrow¹,
4 Mengxiong Wang⁵, Hanyu Su¹, Bianca Forsyth¹, Chi-Wu Chiang⁶, Abhisheak Sharma³, Siva Rama Raju
5 Kanumuri³, Olga A. Guryanova^{1,4}, Jeffrey K. Harrison^{1,4}, Boaz Tirosh⁷, Ronald K. Castellano^{2,4‡}, and Brian K.
6 Law^{1,4‡}

7
8 ¹Department of Pharmacology & Therapeutics, University of Florida, 32610

9
10 ²Department of Chemistry, University of Florida, Gainesville, FL, 32611

11 ³Department of Pharmaceutics, University of Florida, Gainesville, FL, 32610

12 ⁴UF Health Cancer Center, University of Florida, Gainesville, FL, 32610

13 ⁵Department of Radiation Biology, Stanford University, Stanford, CA, 94305

14 ⁶Institute of Molecular Medicine, College of Medicine, National Cheng Kung University, Tainan, Taiwan

15 ⁷Department of Biochemistry, Case Western Reserve University, Cleveland, OH, 44106

16
17 *Equally contributing co-first authors

18 ‡Co-corresponding Authors

21 **Abstract**

22
23
24 New agents are needed that selectively kill cancer cells without harming normal tissues. The TRAIL ligand and
25 its receptors, DR5 and DR4, exhibit cancer-selective toxicity, but TRAIL analogs or agonistic antibodies
26 targeting these receptors have not received FDA approval for cancer therapy. Small molecules for activating
27 DR5 or DR4 independently of protein ligands may bypass some of the pharmacological limitations of these
28 protein drugs. Previously described Disulfide bond Disrupting Agents (DDAs) activate DR5 by altering its
29 disulfide bonding through inhibition of the Protein Disulfide Isomerases (PDIs) ERp44, AGR2, and PDIA1.
30 Work presented here extends these findings by showing that disruption of single DR5 disulfide bonds causes
31 high-level DR5 expression, disulfide-mediated clustering, and activation of Caspase 8-Caspase 3 mediated
32 pro-apoptotic signaling. Recognition of the extracellular domain of DR5 by various antibodies is strongly
33 influenced by the pattern of DR5 disulfide bonding, which has important implications for the use of agonistic
34 DR5 antibodies for cancer therapy. Disulfide-defective DR5 mutants do not activate the ER stress response or
35 stimulate autophagy, indicating that these DDA-mediated responses are separable from DR5 activation and
36 pro-apoptotic signaling. Importantly, other ER stressors, including Thapsigargin and Tunicamycin also alter
37 DR5 disulfide bonding in various cancer cell lines and in some instances, DR5 mis-disulfide bonding is
38 potentiated by overriding the Integrated Stress Response (ISR) with inhibitors of the PERK kinase or the ISR
39 inhibitor ISRIB. These observations indicate that the pattern of DR5 disulfide bonding functions as a sensor of
40 ER stress and serves as an effector of proteotoxic stress by driving extrinsic apoptosis independently of
41 extracellular ligands.

42
43
44

Introduction

45

46 Cancer remains one of the most lethal diseases, making the identification of safer and more effective therapies
47 urgent. Identification of cancer drug targets that are essential for malignant cells, but not normal cells, is key.
48 Targeting proteins involved in the folding and maturation of oncoproteins, but not “house-keeping” proteins,
49 holds great promise. Protein Disulfide Isomerases (PDIs) comprise a family of 22 human enzymes that play
50 essential roles in the folding of secreted and membrane proteins [1]. Previous work showed that PDIs may be
51 favorable targets for anticancer agents [2-6]. However, much of this work focused on canonical PDIs with
52 CXXC active site motifs and little is known about non-canonical PDIs that possess CXXS active site trapping
53 motifs that lack the second, resolving cysteine. Previous work indicated that bicyclic thiosulfonate compounds
54 termed Disulfide bond Disrupting Agents (DDA) bind to the PDIs PDIA1, ERp44, AGR2, and AGR3 through
55 their active site Cys residues [7]. DDAs block client binding to PDIA1 and ERp44 and prevent disulfide-
56 mediated AGR2 dimerization. Further, mutation of the active site Cys residues of ERp44 and AGR2 ablate
57 binding to biotinylated DDAs. Collectively, these results suggest that DDAs inhibit the catalytic activity of
58 PDIA1, ERp44, AGR2, and AGR3 by covalently modifying their active site Cys residues.

59 Importantly, DDAs show significant activity against breast tumors and metastatic lesions in animal
60 models without affecting surrounding stromal cells or normal tissues [8, 9]. Tumor cell death occurred through
61 apoptosis, and DDA-mediated apoptosis was associated with downregulation of the HER-family oncoproteins
62 EGFR, HER2, and HER3 and upregulation and activation of DR5, a receptor for the pro-apoptotic ligand
63 TRAIL. However, significant questions remain regarding DDA modes of anticancer action, determinants of
64 cancer responsiveness to DDAs, and the features controlling DDA safety and metabolic stability. The work
65 presented here was designed to address these questions. The results reveal that DR5 plays a central role in
66 the cancer-selective, pro-apoptotic effects of the DDAs, that DR5 levels and signaling activity through the
67 Caspase 8-Caspase 3 axis are controlled by the state of DR5 disulfide bonding, and that multiple inducers of
68 endoplasmic reticulum protein folding stress alter DR5 disulfide bonding. These observations suggest that DR5
69 functions as both a sensor and effector of proper disulfide bond formation in proteostasis.

70 Results

71
72 *DDA-triggered selective ER retention (sERr) is associated with elevated DR5 levels and signaling:* The DDAs
73 used herein are presented in Fig. 1A. We proposed that DDAs exhibit rapidly reversible covalent bonding to
74 protein thiols by disulfide bond formation, with the exception of the target PDIs that form stable disulfide bonds
75 with DDAs [10]. In further support of this premise, we incubated T47D cell extracts with the biotinylated DDA
76 probe Bio-Pyr-DTDO alone or combined with a 100-fold excess of the unlabeled DDA competitors shown in
77 Fig. 1B. Bands recognized by Bio-Pyr-DTDO were identified as PDIA1, ERp44, and AGR2 by mass
78 spectrometry and immunoblot as reported previously [7]. Endogenous biotinylated proteins are observed in the
79 absence of Bio-Pyr-DTDO treatment (asterisks). As expected, Bio-Pyr-DTDO binding was blocked by the more
80 reactive, less selective DDAs DTDO, D5DO, D7DO, and RBF3. In contrast, the less reactive, more selective
81 DDA tcyDTDO did not affect Bio-Pyr-DTDO binding, nor did the thiol-reactive deubiquitinase inhibitor b-AP15
82 [11]. The thiol-reactive compound *N*-ethylmaleimide prevented Bio-Pyr-DTDO binding to DDA targets. These
83 observations support the selectivity of bicyclic DDAs against a subset of PDIs.

84 Also consistent with previous work, the bicyclic DDAs dFtcyDTDO and dMtcyDTDO increased the
85 levels of DR5, and immunoblot analysis under non-reducing conditions showed an electrophoretic mobility shift
86 of monomeric DR5 and an increase in disulfide bonded oligomeric forms of DR5 (Fig. 1C). A previous study
87 from the Tirosh laboratory showed that under Endoplasmic Reticulum (ER) stress conditions, trafficking of
88 some mis-disulfide bonded transmembrane receptor tyrosine kinases became arrested in the ER through the
89 formation of large disulfide bonded complexes involving ERp44 [12]. This mechanism was termed selective ER
90 retention, or sERr. Since DDAs induce ER stress and inhibit ERp44 client binding [7], we examined whether
91 DDA treatment activates or inhibits sERr. Increasing dFtcyDTDO blocked maturation of MET, an established
92 marker of sERr and also prevented maturation of PCSK9 through its auto-cleavage (Fig. 1D). This was
93 associated with increased expression of the ER stress marker XBP1s. Analysis of the same samples under
94 non-reducing conditions showed that increasing dFtcyDTDO concentrations increased EGFR oligomerization,
95 and elevated levels of monomeric and oligomeric DR5. dFtcyDTDO had a modest effect on PDIA1 client
96 binding. In contrast, dFtcyDTDO blocked the formation of lower molecular mass ERp44 disulfide bonded

97 complexes with clients (red arrows), while very high mass ERp44 complexes (green arrow) were elevated. This
98 observation suggests that DDAs caused sERr. However, the observation that high levels of mis-disulfide
99 bonded monomeric DR5 accumulated suggests that DR5 may evade sERr.

100 The DDA dMtcyDTDO also induced sERr as indicated by near complete blockade of MET maturation
101 (Fig. 2A). This effect was not altered by signaling inhibitors of mTORC1 (rapamycin), Akt (MK2206), EGFR
102 (Gefitinib), or EGFR and HER2 (Lapatinib). The PERK kinase suppresses protein synthesis under ER stress
103 conditions in part through phosphorylation of eIF2 α [12], and previous work [12] showed that sERr is strongly
104 potentiated by PERK inhibition. In MDA-MB-468 cells, Thapsigargin induced a partial block of MET processing
105 that was strongly potentiated by the PERK inhibitor GSK2606414 (hereafter called PERKi) as expected. Since
106 DDAs activate sERr, and sERr is potentiated by PERKi, cell viability studies were performed to examine the
107 effect of DDA/PERKi combination treatment. While PERKi alone had little effect on cell viability, PERKi strongly
108 potentiated dFtcyDTDO cytotoxicity in MDA-MB-468 breast cancer cells (2B, left panel) and WM793 melanoma
109 cells (2B, right panel). sERr was initially investigated primarily in HepG2 hepatoma cells [12], so we compared
110 the combinatorial effects of dMtcyDTDO and PERKi in HepG2 and MDA-MB-468 cells. In both lines PERKi
111 alone had no effect on MET or PCSK9 processing (Fig. 2C). However, PERKi increased the levels of
112 unprocessed MET in both lines and elevated levels of unprocessed PCSK9 in HepG2 cells. This is consistent
113 with PERKi permitting continued synthesis of nascent MET and PCSK9 under ER stress conditions.
114 Combinatorial DDA/PERKi treatment was associated with increased Caspase 8 cleavage, which could explain
115 the enhanced toxicity to cancer cells. PERKi did not strongly potentiate DDA upregulation of DR5, but
116 potentiated Caspase 8 cleavage/activation (Fig. 2D). DR5 knockout partially blunted Caspase 8 cleavage. The
117 compound ISRIB [13] negates the integrated stress response (ISR) by overcoming the effects of
118 eIF2 α phosphorylation [14]. When combined with dMtcyDTDO, ISRIB and PERKi produced similar
119 enhancements in the levels of unprocessed MET and PCSK9 (Fig. 2E). This is consistent with both agents
120 overcoming ISR triggered by DDA treatment. Combinatorial DDA/PERKi activation of Caspase 8 in MDA-MB-
121 468 cells was not altered by forced CDCP1 expression, which disrupts cell-cell adhesion and confers
122 suspension growth [15], (Supplemental Fig. S1A), and PERKi actions were not mimicked by inhibition of
123 eEF2K [6] that controls translation initiation (Supplemental Fig. S1B). Together, these observations suggest

124 that PERKi enhances DDA toxicity to cancer cells by potentiating DR5 pro-apoptotic signaling rather than
125 upregulating DR5 expression.

126

127 *Multiple ER stress inducers alter DR5 disulfide bonding:* Since ERp44 is a DDA target, we examined if ER
128 stress alters DR5 disulfide bonding in the absence of ERp44, or in HepG2 ERp44 knockout cells in which wild
129 type or catalytically null (C29S) versions of ERp44 were reintroduced. The most notable effect was that the ER
130 stressor Thapsigargin and PERKi had little effect alone, but irrespective of the presence or absence of ERp44,
131 Thapsigargin + PERKi decreased DR5 electrophoretic mobility and increased its levels (Fig. 3A). This
132 suggests that while DDAs are sufficient to alter DR5 disulfide bonding alone, other ER stressors may perturb
133 DR5 disulfide bonding, particularly if combined with agents that override the ISR. Consistent with this,
134 treatment of MDA-MB-468 cells with dFtcyDTDO altered DR5 levels and disulfide bonding, while Tunicamycin
135 increased DR5 levels without altering its mobility, and PERKi alone had no discernable effect (Fig. 3B).
136 Tunicamycin + PERKi induced a partial shift in DR5 mobility, similar to that seen with dFtcyDTDO treatment,
137 and this shift was associated with higher Caspase 8 cleavage and more numerous Caspase 3 cleavage
138 products. Unlike DR5, DR4 is *N*-glycosylated. DR4 levels were not changed under any of the conditions, but
139 DR4 mobility was increased by Tunicamycin, presumably due to its deglycosylation.

140 Analysis of the effects of other ER stressors on MDA-MB-468 cells indicated that while PERKi alone
141 had little effect on Caspase 8 cleavage, PERKi potentiated induction of Caspase 8 cleavage by Thapsigargin,
142 Tunicamycin, Cyclosporine A, and Dithiothreitol (Fig. 3C). Increased Caspase 8 cleavage correlated with DR5
143 oligomerization, and in some cases, reduced mobility of monomeric DR5. Immunoblot of MET under reducing
144 conditions showed that dFtcyDTDO and Thapsigargin induced sERr. Tunicamycin + PERKi induction of sERr
145 is difficult to assess given the potentially offsetting effects of deglycosylation and lack of MET proteolytic
146 processing. PERKi caused greater accumulation of unprocessed MET in combination with Thapsigargin than
147 with dFtcyDTDO. Consistent with this observation, protein synthesis assays showed that PERKi increased
148 protein synthesis in the presence of Tunicamycin, but further decreased protein synthesis in the presence of
149 dFtcyDTDO (Fig. 3D). Analysis of the effects of ER stressors on HepG2 cells showed little effect of PERKi or
150 dFtcyDTDO on DR5 levels, while PERKi caused DR5 mobility shifts when combined with Thapsigargin or

151 Tunicamycin (Fig. 3E). Thapsigargin + PERKi caused sERr as assessed by MET processing. Levels of the
152 PERK downstream effector ATF4 increased in response to Thapsigargin, Tunicamycin, and Cyclosporine A. In
153 each case ATF4 upregulation was partially reversed by PERKi.

154 We next compared ER stress responses observed in PERK knockout and control HepG2 cells. In
155 control cells Thapsigargin increased monomeric and oligomeric DR5 levels and PERKi-cotreatment caused
156 upshifting of the long DR5 isoform and increased DR5 oligomerization (Fig. 3F). As expected, PERKi had no
157 discernable effect on the levels or electrophoretic mobility of DR5 in the PERK knockout cells. We consistently
158 observed a smaller band recognized by the PERK antibody in the presence of PERKi + ER stressors. This
159 likely results from Caspase cleavage of PERK since it is decreased by Caspase inhibitor Q-VD-OPH. Due to
160 differences in the responses of MDA-MB-468 and HepG2 cells to the various ER stressors, we examined ER
161 stress-induced changes in DR5 electrophoretic mobility under non-reducing conditions in neuroblastoma (SH-
162 SY5Y), cervical carcinoma (A431), and human mammary epithelial (HMEC) cells. In SH-SY5Y cells,
163 dFtcyDTDO induced an upward DR5 shift. dFtcyDTDO + PERKi did not further slow DR5 mobility, but
164 increased DR5 oligomerization (Fig. 3G). DR5 mobility and oligomerization were most strongly affected by
165 PERKi combined with Thapsigargin or Tunicamycin in the A431 cells. HMECs exhibited the smallest effect of
166 any of the ER stressors on monomeric DR5 levels, but exhibited a low level of DR5 oligomerization when ER
167 stressors were combined with PERKi. Similar analyses in WM793 melanoma cells showed that dFtcyDTDO
168 alone induced DR5 shifts under non-reducing conditions that were not further potentiated by PERKi or ISRIB
169 (Fig. 3H). Thapsigargin, but not Tunicamycin, induced partial DR5 shifts that were accentuated by PERKi.
170 Together, the findings in Figs. 1 and 2 reveal that changes in DR5 disulfide bonding caused by ER stressors
171 differ among various cancer and non-transformed cell lines and that in some cases ER stress alone is
172 sufficient to alter monomeric DR5 mobility and induce its oligomerization, while in other cases, these effects
173 are potentiated by PERKi.

174

175 *EGFR overexpression elevates DDA-induced accumulation of mis-disulfide bonded, monomeric DR5:* Given
176 previous observations that DDAs downregulate HER-family proteins [16], and that EGFR overexpression
177 sensitizes cells to DDA cytotoxic effects [17], we examined if DDAs differentially perturb DR5 disulfide bonding

178 and levels in various cancer lines versus non-transformed cells. The DDAs dMtcyDTDO and dFtcyDTDO did
179 not increase DR5 levels in non-transformed MCF10A mammary epithelial cells, HaCaT human keratinocytes,
180 or the T47D luminal breast cancer cell line (Fig. 4A). In contrast, the DDAs induced robust increases in DR5
181 expression in the MDA-MB-468 and HCC1937 triple-negative breast cancer cell lines. Similarly, while
182 dFtcyDTDO, dFtcyDTDO + PERKi, and Tunicamycin + PERKi reduced DR5 mobility in MDA-MB-468 cells
183 (Fig. 4B), only Tunicamycin + PERKi increased DR5 levels and decreased its mobility in HMECs. Since MDA-
184 MB-468 cells express high EGFR levels [18], we examined if EGFR overexpression is sufficient to confer
185 sensitivity of DR5 to DDA-induced changes in disulfide bonding in MCF10A cells. dFtcyDTDO decreased DR5
186 mobility in the EGFR overexpressing cells, but not the vector control cells (Fig. 4C). ER stressor Cyclosporine
187 A did not induce this effect. Analysis of the disulfide bonding status of the DDA targets AGR2, ERp44, and
188 PDIA1 showed that EGFR overexpression increased levels of disulfide-bonded oligomers of these PDIs as
189 observed previously [7]. AGR2 is secreted by some cells [19-22], so we examined if dFtcyDTDO or
190 Cyclosporine A caused AGR2 secretion. As expected [23], Cyclosporine A caused Cyclophilin B secretion, but
191 AGR2 secretion was not observed under these conditions.

192 Since we previously observed that as with EGFR, MYC overexpression sensitizes cells to DDA-driven
193 apoptosis [7], we examined the effects of MYC on DR5 disulfide bonding. dFtcyDTDO shifted DR5 mobility in
194 MYC overexpressing cells, albeit not to the extent observed with EGFR overexpression (Fig. 4D). GRP78
195 immunoblot indicated that dFtcyDTDO induced a stronger ER stress response in the EGFR and MYC
196 overexpressing cells as compared with the vector control. We previously showed that DDAs selectively
197 upregulate DR5 in a subset of cancer cells and oncogene transformed epithelial lines [7, 8]. The results in Fig.
198 4 show that this DR5 upregulation by ER stressors is associated with changes in the disulfide bonding of the
199 monomeric forms of DR5, and in some cases is associated with disulfide-mediated DR5 oligomerization.

200
201 *DR5 levels and oligomerization states are altered by perturbation of DR5 auto-inhibitory domain disulfides: A*
202 recent study showed that the disulfide bond-rich extracellular domain of DR5 serves to prevent receptor
203 oligomerization and pro-apoptotic signaling in the absence of its ligand TRAIL [24]. A more recent article
204 narrowed down the DR5 autoinhibitory domain to a positive patch involving residues R154, K155, and R157

[25]. Based on a crystal structure [26], these basic residues share a common orientation due to two disulfide bonds, C156-C170 and C139-153 (Fig. 5A). We hypothesized that loss of these two disulfide bonds may disrupt the auto-inhibitory domain, culminating in DR5 clustering and activation of Caspase 8-Caspase 3-mediated apoptosis independently of TRAIL or DDA treatment. This hypothesis was tested by doxycycline-inducible expression of wild type and disulfide-defective DR5 point mutants. High-level inducible expression of the long form of wild type DR5 required induction by doxycycline combined with DDA treatment as described previously [8], while mutation of one or both of the Cys residues of the C160-C178 disulfide bond conferred high level DR5 expression in the absence of DDA treatment, as did the C81S mutation (Fig. 5B). Interestingly, DDA treatment still caused an upward shift in these mutants under reducing conditions suggesting that DDAs may disrupt multiple DR5 disulfide bonds. The DR5 disulfide-defective mutants, but not wild type DR5, also caused formation of high molecular weight DR4 oligomers in the absence of DDA treatment suggesting that endogenous DR4 may co-aggregate with ectopic, mis-disulfide bonded DR5 oligomers.

We next examined if Caspase activation limits expression of DR5[C153S], DR4, or the murine TRAIL receptor (mDR5) by inhibiting Caspases with Q-VD-OPH [27]. Q-VD-OPH increased the inducible expression of all three receptors and prevented formation of the p18 fragment of Caspase 8, but not the p41/p43 fragment (Fig. 5C). This likely indicates that Q-VD-OPH does not inhibit receptor-driven Caspase 8 autocleavage, but inhibits the previously described [28] Caspase 3 cleavage of Caspase 8. We further examined the relationship between DR5 and DR4 oligomerization and Caspase activation using C-terminal DR5 or DR4 deletion constructs since such mutants were previously shown incapable of coupling to Caspase 8 activation [29]. Doxycycline and doxycycline + dMtcyDTDO produced similar effects on the levels of the wild type and mutant DR5 and DR4, although the mutants were incapable of activating the Caspase 8-Caspase 3 cascade (Fig. 5D). Since DDAs cause ER stress, we examined if ER stress is independent of DR5-mediated Caspase activation. dMtcyDTDO upregulated ER stress markers, decreased AKT phosphorylation, and increased disulfide-mediated EGFR oligomerization irrespective of Caspase activation (Fig. 5E).

DR5 mutants lacking the disulfide bonds that form the positive patch exhibit high expression and oligomerization in the absence of DDA treatment, unlike wild type DR5 (Fig. 5F). Upregulation of DR5 by disruption of positive patch Cys residues was observed with two antibodies that recognize the C-terminal

232 (#8074) or N-terminal (sc-166624) regions of DR5, although the latter antibody exhibited a strong binding
233 preference for oligomeric DR5 isoforms over monomeric DR5 (Fig. 5G). The PhosphoSite database
234 (Phosphosite.org) lists K245 as a major site of DR5 ubiquitination. Mutation of this site to Arg modestly
235 increased receptor levels in the doxycycline and doxycycline + DDA treated samples, but did not mimic the
236 ability of the C-S mutations to exhibit high level expression in the absence of DDA treatment. In summary, the
237 results in Fig. 5 indicate that individual mutation of several different DR5 disulfides, including the positive patch
238 disulfides, is sufficient for high level expression of DR5 and activation of Caspases independent of DDA
239 treatment or ER stress. Further, stabilization of mis-disulfide bonded DR5 does not require Caspase activation,
240 but, activation of Caspase 8 by mis-disulfide bonded DR5 requires its C-terminus that is necessary for DISC
241 formation [29].

242
243 *DDAs activate autophagy and autophagy inhibitors potentiate DDA-induced DR5 accumulation:* Proteasomal
244 degradation (ERAD) and autophagy are important modes for the disposal of misfolded proteins. However, the
245 fate of mis-disulfide bonded, aggregated proteins in the secretory pathway is underexplored. Since DDAs
246 induce ER stress [17], and ER stress frequently activates autophagy [30], we examined if DDAs stimulate
247 autophagy. dFtcyDTDO treatment induced an upward DR5 shift in a concentration-dependent manner. GPR78
248 expression and autophagy marker LC3 lipidation were both increased to maximal levels at the lowest
249 dFtcyDTDO concentration tested (Fig. 6A). Treatment with the autophagy/lysosome inhibitor Bafilomycin A1
250 increased levels of monomeric and oligomeric DR5 isoforms in the absence of DDA treatment (Fig. 6B).
251 Similar studies employing the autophagy/lysosome inhibitor Chloroquine showed increased DR5 levels and
252 accumulation of oligomeric EGFR compared with vehicle treatment. Combining dFtcyDTDO with Chloroquine
253 or PERKi increased DR5 levels and Caspase 8 cleavage over that observed with dFtcyDTDO alone (Fig. 6C).
254 Cell viability assays of cells treated as in Fig. 6C showed that combining dFtcyDTDO with either PERKi or
255 Chloroquine reduced viability more than dFtcyDTDO, and combining the three agents decreased viability the
256 most (Fig. 6D). An inhibitor of the autophagy PI3-kinase VPS34 (VPS34i, [31]) increased DR5 expression to a
257 similar extent as Bafilomycin, and combining dFtcyDTDO with either VPS34i or Bafilomycin increased
258 expression of monomeric DR5 more than each individual treatment (Fig. 6E). Of these treatments, only

dFtcyDTDO or the dFtcyDTDO-containing treatments upshifted monomeric DR5. The strong accumulation of upshifted monomeric DR5 caused by autophagy inhibitors suggests that autophagy plays a role in degrading mis-disulfide bonded DR5.

DDAs upregulate DR5 paralog DcR2: The pro-apoptotic TRAIL receptors DR4 and DR5 share conserved disulfide-rich domains with the TRAIL decoy receptors DcR1 and DcR2 that bind TRAIL, but cannot activate Caspases. Specifically, the DR5 autoinhibitory domain is largely conserved with DR4, DcR1, and DcR2 (Fig. 7A). We considered that DDAs might stabilize DcR1 or DcR2 in a similar manner as DR5. Since we previously found that the prolyl isomerase inhibitor Cyclosporine A potentiated DDA cytotoxic effects [9], we examined Cyclosporine A effects on the levels of decoy receptors. We did not detect DcR1 in the cell lines examined, but observed upregulation of DcR2 after dFtcyDTDO treatment (Fig. 7B). We also observed that Cyclosporine A, but not FK606, which inhibits a different family of prolyl isomerases, decreased DDA upregulation of DcR2, but not DR5. dFtcyDTDO increased DcR2 levels more at low concentrations than high concentrations in some experiments, but irrespective of the pattern of DcR2 upregulation by dFtcyDTDO, it was blocked by co-treatment with Cyclosporine A (Fig. 7B-D). Quantitation of band intensities revealed that Cyclosporine A treatment potentiated the effects of low (310 nM) dFtcyDTDO concentration on DR5 oligomerization (Fig. 7E, left panel) and decreased DcR2 upregulation by dFtcyDTDO (Fig. 7E, right panel).

DR5 bonding status influences antibody recognition, but not trafficking to the cell surface: Since sERr prevents some transmembrane receptors from reaching the cell surface [12] and DR5 was shown to be activated in the Golgi by binding to aggregated proteins [32], we examined DR4 and DR5 cell surface labeling by flow cytometry. Using the Clone DJR2-4 (7-8) antibody for flow cytometry analyses, Doxycycline induction of the wild type, C153S, and C156S mutants showed DR5 increased cell surface labeling, however co-treatment with dFtcyDTDO decreased apparent DR5 surface localization (Fig. 8A, upper panel). DR4 flow cytometry studies showed that doxycycline increased DR4 surface levels and this was not altered by dFtcyDTDO co-treatment. Since recognition of DR5 by the flow cytometry antibody could be hindered by changes in DR5 disulfide bonding, we examined levels of DR5 and its disulfide bonding mutants using three different commercially

286 available antibodies (Fig. 8B). The #8074 antibody directed against the cytoplasmic, C-terminal portion of DR5
287 recognized all of the DR5 proteins, including the monomeric and oligomeric forms of DR5. As shown here (Fig.
288 5) and elsewhere [8], wild type DR5 was only maximally expressed in cells induced with doxycycline and
289 treated with DDAs. The sc166624 DR5 antibody directed against the N-terminal cysteine-rich region
290 preferentially recognized the oligomeric forms of DR. In contrast, Clone DJR2-4 (7-8) directed toward the N-
291 terminal cysteine-rich portion of DR5 did not recognize the C119S/C137S DR5 mutant, but bound the C153S,
292 C156S, C160S, and C160S/C178S DR5 mutants. However, dFtcyDTDO treatment ablated DR5 recognition by
293 this antibody. These observations suggest that binding of Clone DJR2-4 (7-8) antibody is sensitive to DR5
294 disulfide bonding, which is altered by DDA treatment. Since this antibody is commonly used for DR5 labeling in
295 flow cytometry studies and multiple ER stressors, including DDAs, alter DR5 disulfide bonding, lack of signal
296 with this antibody may be indicative of changes in DR5 disulfide bonding rather than DR5 downregulation or
297 internalization.

298 Previous work showed that DDA treatment increased surface localization of DR5 as measured by biotin
299 labeling [7]. The same approach was used to examine the localization of the DR5 mutants to the cell surface.
300 The results showed that the C119S/C137S, C153S, and C156S mutants trafficked to the cell surface,
301 particularly in the context of DDA treatment (Fig. 8C). Under these conditions, expression of DR5 disulfide
302 bonding mutants did not elicit an ER stress response as indicated by the markers GRP78, XBP1s, and PERK
303 activation (phosphorylation). However, dFtcyDTDO activated all these indicators of ER stress. A similar cell
304 surface biotinylation experiment showed trafficking of wild type and mutant DR5 to the cell surface. Surface
305 localization of the C119S/C137S and C153S DR5 mutants occurred in both the presence or absence of
306 dFtcyDTDO or the ER stress inducer Cyclosporine A (Fig. 8D). Expression of mis-disulfide bonded DR5
307 mutants did not upregulate the ER stress or autophagy markers GRP78, or LC3, respectively, but DDA
308 treatment upregulated both markers. Together, these results indicate that under conditions where DR5
309 disulfide bonding is perturbed by either mutagenesis or DDA treatment, DR5 traffics to the cell surface. This is
310 consistent with previous work showing that DDA treatment increases cancer cell sensitivity to the DR4/5 ligand
311 TRAIL [8].

313 *DDA safety and identification of a metabolically stable DDA analog*: Previous work with the DDAs RBF3 [16]
314 and tcyDTDO [8] did not reveal evidence of toxicity under conditions in which they induce the death of primary
315 and metastatic breast cancer cells in mouse models. We also examined the metabolism of the DDA tcyDTDO
316 by liver microsomes [9], but did not present analyses of the stability of dMtcyDTDO and dFtcyDTDO toward
317 metabolism in liver and intestinal microsomes. Recent work demonstrated the activity of both dMtcyDTDO and
318 dFtcyDTDO in mouse models of breast cancer [33], but did not examine the effects of these compounds on
319 normal tissues such as the liver or hematopoietic cells. Examination of breast tumor tissue from mice treated
320 with vehicle or 10 mg/kg dMtcyDTDO showed extensive death of tumor tissue in the dMtcyDTDO-treated, but
321 not the vehicle-treated mice (Fig. 9A, upper panels). Liver tissues from vehicle or dMtcyDTDO-treated mice
322 were indistinguishable (Fig. 9A, lower panels). Analysis of complete blood cell counts from tumor-bearing mice
323 treated with vehicle or 10 mg/ml dMtcyDTDO were in the normal range for healthy mice (Supplemental Table:
324 S1). The apparent decrease in platelets across the samples was likely due to partial clotting prior to analysis.

325 Stability studies in human liver microsomes supplemented with NADPH showed that FtcyDTDO was
326 metabolically stable ($t_{1/2} > 60$ min), while tcyDTDO, and dMtcyDTDO metabolized by phase I enzymes with
327 half-lives of 11.9, and 47.9 min, respectively. Similar studies employing human intestinal microsomes showed
328 that the half-life of all three DDA compounds exceeded 60 min. Although more thorough analysis of these
329 DDAs is needed, studies performed to date indicate that dFtcyDTDO has a more favorable metabolic stability
330 profile than tcyDTDO or dMtcyDTDO.

331

332

333 Discussion

334 Previous work showed that the DDA compounds induce ER stress, which is associated with high-level DR5
335 expression and disulfide-mediated oligomerization [8, 17, 34]. Further, mutational disruption of a subset of DR5
336 disulfide bonds was demonstrated to stabilize DR5 and trigger disulfide-mediated DR5 oligomerization.
337 However, the relationship between the DDA-induced ER stress response and DDA effects on DR5 were
338 unexplored. The results presented here show that individual mutational disruption of a total of five of the seven
339 DR5 disulfide bonds each causes the same DR5 stabilization, including the disulfides within the previously
340 described auto-inhibitory domain [24, 25]. The observation that DDAs still induce a mobility shift of monomeric
341 disulfide point mutants of DR5 suggests that while loss of individual disulfide bonds is sufficient to stabilize
342 DR5 and promote pro-apoptotic signaling, DDAs disrupt multiple DR5 disulfide bonds.

343 Numerous studies have demonstrated transcriptional regulation of DR5 through a PERK-ATF4-CHOP-
344 DR5 pathway [35, 36]. In this model, PERK inhibition is predicted to block DR5 upregulation by ER stress. Our
345 previous studies in breast cancer lines found little effect of knocking out or overexpressing CHOP on DR5
346 levels, suggesting that other DR5 regulatory mechanisms exist [8]. We found here that PERK inhibition
347 potentiated DR5 pro-apoptotic signaling, but only modestly increased DR5 levels. A report showed that DR5 is
348 activated by binding to misfolded proteins in the Golgi [32], so PERKi might elevate DR5 oligomerization
349 through this mechanism. Alternatively, overriding ISR may activate DR5 by increasing protein folding flux under
350 ER stress conditions and surpass the ability of the DDA targets ERp44, PDIA1, and AGR2 to catalyze disulfide
351 bond formation or their functions in protein folding checkpoints. A recent report showed that breast cancer
352 metastases exhibit elevated ER stress and are responsive to a new, more selective PERK inhibitor [37]. This
353 along with our previous study showing DDA activity against breast cancer metastases [8] provides a rationale
354 for DDA/PERKi combination therapy for the treatment of metastatic breast cancer. Likewise, the observation
355 that Cyclosporine A blocks DDA-induced upregulation of DCR2 further supports the previous contention [9]
356 that DDA/Cyclosporine co-treatment may exhibit enhanced efficacy against breast malignancies.

357 Overexpression of the EGFR or MYC oncoproteins was shown to sensitize cells to DDA cytotoxic
358 effects, but the underlying mechanisms were not investigated [8]. Results presented here show that EGFR or
359 MYC overexpression permits DDA perturbation of DR5 disulfide bonding that is not observed in vector control

360 non-transformed MCF10A mammary epithelial cells. This may partially explain the ability of DDAs to mimic the
361 cancer-specific cytotoxic effects of the DR5/4 ligand TRAIL. Interestingly, expression of disulfide bonding
362 mutants of DR5 does not trigger an ER stress response or activate autophagy. Further, mis-disulfide bonded
363 DR5 traffics to the cell surface, consistent with the previous observation that DDAs synergize with TRAIL to kill
364 cancer cells [8]. The present results extend previous work on the relationship between ER stress and DR5
365 activation by showing that in addition to DDAs, other ER stressors, including Tunicamycin and Thapsigargin,
366 can alter DR5 disulfide bonding in a manner that is potentiated in some cases by PERKi co-treatment. A
367 subject of ongoing investigation is why ER stressors that alter DR5 disulfide bonding do not have the same
368 effect on its paralog DR4. This may relate to the different N- and O-glycosylation patterns observed for these
369 receptors [38-41], or regulation of DR4 and DR5 stabilities by different E3 ubiquitin ligases [42-44]. Together,
370 our work [7, 8, 17] and that of others [32], suggest that DR5 has evolved as a direct sensor and effector of ER
371 stress/protein misfolding and that ER stress can activate DR5 through transcriptional mechanisms and at the
372 protein level through altered DR5 disulfide bonding and DR5 binding to misfolded proteins. Importantly, DR5
373 exhibits a TRAIL-independent gain of function under these conditions that inactivate a wide variety of other
374 transmembrane oncoproteins, including EGFR and MET.

375 DDA studies have been performed largely in breast cancer cell lines, therefore it will be critical to
376 determine the importance of these DDA-driven effects in non-transformed cells and across other tumor types.
377 This DDA cancer selectivity is further supported by the Broad Institute's Dependency Map (DepMap;
378 depmap.org/portal/). Of the 22 human disulfide isomerases, only four, ERp44, AGR2, AGR3, and TMX1, are
379 considered as "strong dependencies" in the DepMap, and our studies have shown DDAs to inhibit three of
380 these, ERp44, AGR2, and AGR3. It is possible that the client proteins of ERp44, AGR2, and AGR3 vary with
381 tumor type. As an example, out of 17,347 genes in the DepMap CRISPR screen, the colon cancer lines C80,
382 COLO205, LS513, and SNUC4 rank AGR2 as the first, fourth, third, and fifth most important gene,
383 respectively. Interestingly, ERN2 encodes the IRE1 α homolog IRE1 β whose expression is restricted to Goblet
384 cells. The DepMap lists IRE1 β as the top predictor of AGR2 dependence. Two recent reports show that AGR2
385 functions as an inhibitor of IRE1 β that overcomes the cytotoxic effects of this enzyme [45], and that the active
386 site Cys81 of AGR2 is required for IRE1 β inhibition [46, 47]. It will be important to determine if DDAs exhibit

387 anticancer activity against tumor lines in which AGR2 is required to prevent IRE1 β -mediated cancer cell death.

388 This is an area of active investigation by our team.

389 More generally, DDAs may serve as important tools for investigating disulfide bonding quality control in
390 the secretory pathway. Significant interest has recently focused on DDAs and similar compounds for their
391 ability to function in transport across cell membranes in thiol-mediated uptake [48] and as redox-sensitive
392 probes [49] indicating the value of six membered cyclic dichalcogenides for diverse biological applications. As
393 an inhibitor of ERp44, DDAs may override two key protein disulfide bonding checkpoints, the retrograde Golgi-
394 ER recycling of secretory proteins discovered by Sitia and Colleagues [50-55], and the selective ER retention
395 mechanism of some receptor tyrosine kinases discovered by Tirosh and Colleagues [12]. Based on these new
396 mechanistic insights and molecular and pharmacological tools, the stage is set to investigate the molecular and
397 biological functions of the non-canonical PDIs, and strongly selective cancer dependencies, ERp44, AGR2,
398 and AGR3.

399

400 **Materials and Methods**

401 **Cell culture, preparation of cell extracts, and immunoblot analysis**

402 MCF10A cells were cultured in a humidified incubator set at 37°C containing 5% CO₂ as described previously
403 [56]. All other cell lines were grown in Dulbecco's Modified Eagle's Medium (GE Healthcare Life Sciences,
404 Logan, UT) with 10% fetal bovine serum (10% FBS–DMEM). A431, AsPC1, HaCaT, HCC1937, HepG2,
405 HMEC, MCF10A, MDA-MB-468, SH-SY5Y, and T47D were purchased from American Type Culture Collection
406 (ATCC) (Manassas, VA). SUM149pt was purchased from Applied Biological Materials, Inc. (Richmond, BC,
407 Canada). ERp44 and PERK knockout HepG2 cell lines were described previously [12]. WM793 cells were
408 kindly provided by Dr. W. Douglas Cress, Moffitt Cancer Center. Generation of the MCF10A/Vector,
409 MCF10A/EGFR and MCF10A/MYC cell lines is described in previous work [8]. Derivation of the HCl-
410 012/LVM2/LR10 cell line is described in previous work [8, 9]. Generation of DR5 knock out MDA-MB-468 cells
411 and MDA-MB-468 cells stably expressing DR5 using the Tet-ON system is previously described [8].
412 Generation of the MDA-MB-468 cells stably expressing CDCP1 or vector control is described in previous work
413 [15].
414

415 Cell lysates were prepared as described in a previous publication [57]. Immunoblot analysis was
416 performed employing the following antibodies purchased from Cell Signaling Technology (Beverly, MA) [Akt,
417 #4691; P-Akt[T308], #13038; ATF4, #11815; CDCP1, #13794; Cleaved Caspase 3, #9664; Cleaved Caspase
418 8, #9496; Cyclophilin B, #43603; DCR2, #8049; DR4, #42533; DR5, #8074; eE2F, #2332; P-eE2F[T56],
419 #2331; GRP78, #3177; HER3, #4754; LC3, #3868; MET, #3127; PARP, #9532; PCSK9, #55728; PDIA1,
420 #3501; PERK, #5683; and XBP1s, #12782], from Santa Cruz Biotechnology (Santa Cruz, CA) [Actin, sc-
421 47778; AGR2/3, sc-376653; AGR3, sc-390940; c-Myc (9E10), sc-40; EGFR, sc-373746; ERp44, sc-393687;
422 PDIA6, sc-365260; and pY99, sc-7020], and from Rockland Immunochemicals, Inc. (Limerick, PA),
423 Streptavidin-Alkaline Phosphatase conjugated (SA-AP), S000-05.
424

425 **Quantitative Analysis of Immunoblot Results**

426
427 Protein levels in immunoblots were quantified using Adobe Photoshop (Berkeley, CA) and ImageJ (NIH,
428 Bethesda, MD), as previously described [58], followed by normalization to Actin as a loading control.

429

430 **Materials**

431 Reagents were purchased from the following companies: Tunicamycin and Chloroquine: Sigma-Aldrich (St.
432 Louis, MO); Thapsigargin: AdipoGen (San Diego, CA); Lapatinib: Selleck Chemicals (Houston, TX);
433 Doxycycline: Enzo Life Science (Farmingdale, NY); TORIN1, and dithiothreitol (DTT): TOCRIS Bioscience
434 (Minneapolis, MN); Cyclosporine A (CsA): Biorbyt (Duran, NC); Rapamycin and PERK Inhibitor I
435 (GSK2656157): Calbiochem (Burlington, Massachusetts); Bafilomycin A1, Gefitinib, ISRIB, MK2206, and Q-
436 VD-OPH: Cayman Chemical (Ann Arbor, MI); *N*-ethylmaleimide (NEM): Thermo Fisher Scientific (Grand
437 Island, NY); eEF2K inhibitor (A-484954) and VPS34 inhibitor Vps34-IN-1: MedChemExpress (Monmouth
438 Junction, NY); FK506: InvivoGen (San Diego, CA); b-AP15: MedKoo Biosciences (Chapel Hill, NC).

439

440 **Tumor studies and histochemical analysis**

441 012/LVM2/LR10 xenograft tumor studies were carried out in adult female NOD-SCID- γ (NSG) mice, as
442 described in a previous publication [9]. After the development of palpable tumors (approximately 4 mm³), mice
443 were randomly assigned to two treatment groups: DMSO (Vehicle) and 10 mg/kg dMtcyDTDO). Mice were
444 treated every weekday for twenty days by intraperitoneal injection, administering 50 μ L per injection. At the end
445 of the twenty-day period, tissue samples were collected and fixed in 4% paraformaldehyde/Phosphate-
446 Buffered Saline (PBS), followed by paraffin-embedding, sectioning and staining with hematoxylin and eosin
447 (H&E) by the University of Florida Molecular Pathology Core (<https://molecular.pathology.ufl.edu/>).
448 Prior to endpoint, peripheral blood was collected by facial vein puncture into EDTA-treated tubes; complete
449 blood cell counts (CBCs) were obtained using an Element HT5 fully automated hematology analyzer (Heska,
450 Loveland, CO).

451

452 **Disulfide Bond-mediated Oligomerization**

453

454 Disulfide bond-mediated oligomerization under non-reducing conditions was analyzed as described in previous
455 work [7].

456

457 **Vector Construction**

458 In order to construct the Tet-DR4 expression vector, DR4 (Addgene plasmid #61382) was amplified using the
459 following primers: 5'-TTTTATCGATCACCATGGCGCCCGTCGCCGTCTGG-3' and

460 5'-TTTTGGATCCTCACTCCAAGGACACGGCAG-3' and cloned into the pRetroX-TetOne-Puro vector with a
461 modified cloning site that incorporates Not I, Bcl I, and Cla I sites 5' to the BamH I site (Clontech, Mountain
462 View, CA, USA).

463 The initial mutations of C81S, C119S and C160S in DR5 were performed in pcDNA3 with QuikChange
464 mutagenesis and the following primers, respectively: 5'-

465 CCAGCCCCTCAGAGGGATTGAGTCCACCTGGACACCATATC-3- and 5'-

466 GATATGGTGTCCAGGTGGACTCAATCCCTCTGAGGGGCTGG-3', 5'-

467 GCTTGCGCTGCACCAGGAGTGATTCAGGTGAAGTGG-3' and 5'-

468 CCACTTCACCTGAATCACTCCTGGTGCAGCGCAAGC

469 -3' and 5'- CGGAAGTGCCGCACAGGGAGTCCCAGAGGGATGGTCAAGG -3' and 5'-

470 CCTTGACCATCCCTCTGGGACTCCCTGTGCGGCACTTCCG

471 -3'. Mutations were verified by sequencing. The following primers were used to add a 5'-EcoRI and a
472 3'-BamHI site to C81S, C119S and C160S DR5 by PCR amplification: 5'-

473 TTTTGAATTCCACCATGGAACAACGGGGACAGAAC-3' and 5'-

474 TTTTGGATCCTTAATGATGATGATGATGATGGGACATGGCAGAGTCTGC-3'. The C119S and

475 C160S DR5 mutants were subsequently cloned into the EcoRI and BamHI sites of pRetroX-TetOne-
476 Puro vector (Clontech, Mountain View, CA, USA). Mutation of the DR5 C94 was produced in the DR5

477 C81S construct to produce the DR5 C81S/C94S using QuikChange mutagenesis and the following
478 primers: 5'-CATATCTCAGAAGACGGTAGAGATAGCATCTCCTGCAAATATGGACAGG-3' and 5'-

479 CCTGTCCATATTTGCAGGAGATGCTATCTCTACCGTCTTCTGAGATATG-3'. Mutation of the DR5

480 C137S was introduced into the DR5 C119S construct to produce the DR5 C119S/C137S using

481 QuikChange mutagenesis and the following primers: 5'-

482 CCACGACCAGAAACACAGTGAGTCAGTGCGAAGAAGGCACCTTC -3' and 5'-
483 GAAGGTGCCTTCTTCGCACTGACTCACTGTGTTTCTGGTCGTGG -3'. The C178S mutation of
484 DR5 was introduced into the DR5 C160S construct to produce the DR5 C160S/C178S using
485 QuikChange mutagenesis and the following primers: 5'-
486 CACCCTGGAGTGACATCGAAAGTGTCCACAAAGAATCAGGTAC -3' and 5'-
487 GTACCTGATTCTTTGTGGACACTTTTCGATGTCCTCCAGGGTG-3'. The C153S and C156S
488 mutations of DR5 were produced using QuikChange mutagenesis and the following primers,
489 respectively: 5'-GAAGAAGATTCTCCTGAGATGAGCCGGAAGTGCCGCACAGGG-3' and 5'-
490 CCCTGTGCGGCACTTCCGGCTCATCTCAGGAGAATCTTCTTC-3' and 5'-
491 CTCCTGAGATGTGCCGGAAGAGCCGCACAGGGTGTCCCAGAGGG-3' and 5'-
492 CCCTCTGGGACACCCTGTGCGGCTCTTCCGGCACATCTCAGGAG-3'. The K245R DR5 mutation
493 was produced by QuikChange Mutagenesis and the following primers: 5'-
494 GTCCTTCCTTACCTGCGAGGCATCTGCTCAGGT-3' and 5'-
495 ACCTGAGCAGATGCCTCGCAGGTAAGGAAGGAC-3'. Tet-DR5 [Δ C41] was produced by amplifying
496 DR5 by PCR, adding 5'-EcoRI and 3'-BamHI sites using the following primers: 5'-
497 TTTTGAATTCCACCATGGAACAACGGGGACAGAAC-3' and 5'-
498 TTTTGGATCCTTACTTGTCGTCATCGTCTTTGTAGTCGACAGAGGCATCTCGCCCGG-3' followed
499 by cloning into the EcoRI and BamHI sites of the pRetroX-TetOne-Puro vector. The Tet-DR4[Δ C43]
500 was produced by amplifying DR4 by PCR, adding 5'-Clal and 3'-BamHI sites using the following
501 primers: 5'-TTTTATCGATCACCATGGCGCCCGTCCCGTCTGG-3' and 5'-
502 TTTTGGATCCTTACTTGTCGTCATCGTCTTTGTAGTCGATCGAGGCGTTCCGTCCAGTTTTG-3'
503 followed by cloning into the Clal and BamHI sites of the pRetroX-TetOne-Puro vector.

504 In order to clone ERp44, total RNA from T47D cells was extracted with TRIzol Reagent
505 (Invitrogen, Waltham, MA USA) according to the manufacturer's protocol. Total cellular RNA was
506 reverse transcribed to synthesize first-strand cDNA using the PCR conditions listed: 25 °C for 10 min,

42 °C for 30 min, and 95 °C for 5 min. DNA encoding ERp44 was subsequently amplified using the following primers: 5'- TTTTGGATCCCACCATGCATCCTGCCGTCTTCC-3' and 5'- TTTTCTCGAGTTAAAGCTCATCTCGATCCCTC-3'. The PCR fragment encoding ERp44 was cloned into the 5' BamHI and 3' XhoI sites of the pMXs-IRES-Blasticidin retroviral vector (RTV-016) (Cell Biolabs, Inc., San Diego, CA USA). The following primers were used to produce the C29S mutation of ERp44 using QuikChange mutagenesis: 5'- CTTTAGTAAATTTTTATGCTGACTGGAGTCGTTTCAGTCAGATGTTG-3' and 5'- CAACATCTGACTGAAACGACTCCAGTCAGCATAAAAATTTACTAAAG-3.' All mutations were verified by sequencing.

MTT Cell Viability Assays

In order to evaluate cell viability, cells were plated at 7,500/well in 96-well plates and incubated at 37°C for 24h. Cells were subsequently treated with various compounds for 72 h at 37°C. Following removal of the cell media, cells were incubated with 0.5 mg/ml MTT (3-(4,5-dimethylthiazol-2-yl)-2,5-diphenyltetrazolium bromide) (Biomatik, Wilmington, DE, United States) in PBS at 37°C for 1 h. The MTT solution was subsequently removed and the MTT formazan product was dissolved in 100 µl of DMSO, followed by measurement of MTT formazan absorbance (570 and 690 nm) in a plate reader.

Protein Synthesis Assays

Leucine incorporation into proteins was assayed using ³H-Leucine (cat. # NET460001MC) obtained from Perkin Elmer (Waltham, MA), as described in a previous publication [33].

Chemical Synthesis of DDAs

The DDAs presented in Fig. 1A. were prepared based on existing literature procedures from our team and others. RBF3, D5DO, and D7DO were obtained according to the methods described by Field and colleagues [59, 60].

DTDO was synthesized as we described previously [16], as well as tcyDTDO [9], dMtcyDTDO and dFtcyDTDO [61], and Bio-Pyr-DTDO [7].

Metabolic stability using rat and human liver and intestinal microsomes

To understand the rate of metabolism of compounds across species the *in vitro* metabolic stability of each compound was performed using liver and intestinal microsomes from rats and humans in triplicate. Verapamil was used as a positive control to check the activity of the microsomes. The incubation mixtures consisted of liver or intestinal microsomes (1 mg /ml protein for liver microsomes and 0.5 mg/ml protein for intestinal microsomes), substrate (10 μ M), and NADPH (1 mM) in a total volume of 0.2 ml potassium phosphate buffer (50 mM, pH 7.4). Reactions were initiated with the addition of NADPH and kept in an incubator shaker at 37°C. Aliquots of 20 μ l were collected at 0, 5, 10, 15, 30, 45, and 60 min and mixed with 100 μ l of acetonitrile with formic acid (0.1% v/v) containing phenacetin (50 ng/ml; internal standard) for the termination of the reaction. The samples were then vortex mixed and filtered through a 0.45 μ m PTFE Solvinert membrane filtration plate under centrifugation at a speed of 2000 \times g for 5 min at 4°C. The filtrates were subjected to UPLC-MS/MS analysis.

The intrinsic clearance of the compounds was calculated using a half-life employing the 'substrate depletion' approach. The apparent half-life was calculated from the pseudo-first-order rate constants obtained by linear regression of log (concentration) and time plots. The *in vitro* intrinsic clearance for compound was estimated using the formula:

$$t_{1/2} = \ln(2)/k$$

$$Cl_{int} (\mu L/min/mg \text{ protein}) = \frac{0.693}{t_{1/2}} \times \frac{V_{\text{incubation in } \mu L}}{\text{Protein Concentration in mg}}$$

Where k is the slope of the line obtained by plotting the natural logarithmic of the percentage of parent remaining versus time and V is the volume of incubation.

556 The *in vitro* intrinsic clearance from rat and human liver microsomes were scaled to whole-organ
557 (hepatic) *in vivo* intrinsic CL ($CL_{int, H}$) using the scaling factors available in the literature using equation
558 [62]:

$$559 \quad Cl_{int, H} \text{ (mL/min*kg)} = \frac{0.693}{t_{1/2} \text{ (min)}} \times \frac{\text{Volume of incubation (mL)}}{\text{Protein in incubation (mg)}} \times \frac{\text{Liver weight (g)}}{\text{Body weight (kg)}} \times SF$$

560 The scaling factor used for the rat was 45 (45 mg microsomal protein/g liver) and liver weight (g) per
561 kg body weight was 40 g/kg while for human scaling factors was 29 (29 mg microsomal protein/g
562 liver) and liver weight (g) per kg body weight was 24 g/kg [63, 64].

563

564 **LC-MS/MS analysis:**

565 UPLC-MS/MS analysis was carried out using a Waters Acquity Class I Plus UPLC coupled
566 with a Waters Xevo TQ-S Micro triple quadrupole mass spectrometer. The chromatographic
567 separation was achieved using Acquity UPLC CSH C18 column (2.1 mm x 50 mm, 1.7 μ m) using the
568 mobile phase consisting of 0.1% formic acid (A) – methanol (B) with a gradient program of 80 % A
569 held for 0.5 min, then decreased A to 65% reaching 1.0 min and further decreased to 40 % A by 2.5
570 min and held at 40 % until 3.0 min, then sharply decreased back to the initial conditions by 3.1 min
571 and maintained until 3.5 min. The column and autosampler temperatures were kept at 50 °C and 4
572 °C, respectively. The mobile phase was delivered at a flow rate of 0.35 mL/min and the injection
573 volume was set to 2 μ L. The MassLynx software version 4.2 was used for instrument control and
574 TargetLynx for data analysis. The mass spectrometer was operated in positive ion mode and
575 detection of the ions was performed in the multiple reaction monitoring (MRM) mode. The monitored
576 ion transitions (m/z) and instrument conditions can be seen in Table 1. Each compound was
577 monitored using two precursor-to-daughter ion transition pairs, one as a quantifier and another as a
578 qualifier to get better selectivity for each compound. The ion spray voltage was set at 3000 V, the
579 desolvation temperature was 400 °C, the desolvation gas flow was 850 L/h, and the cone gas flow
580 was 50 L/h.

581 Table 1. Mass parameters for tcyDTDO, dMtcyDTDO, dFtcyDTDO, and internal standard (IS)

Compound	Parent (<i>m/z</i>)	Daughter (<i>m/z</i>)	Cone (V)	Collision (V)	Type
tcyDTDO	207.16	81.03	46	24	Qualifier
tcyDTDO	207.16	109.02	46	14	Quantifier
dFtcyDTDO	243.10	105.00	44	20	Qualifier
dFtcyDTDO	243.10	125.10	44	16	Quantifier
dMtcyDTDO	267.10	139.10	34	11	Qualifier
dMtcyDTDO	267.10	235.00	34	4	Quantifier
Phenacetin	180.11	110.02	34	20	IS

582

583 Flow Cytometry Analysis

584 Cells were lifted from plates using cell scrapers and washed in ice cold PBS. Single cell suspensions were
585 prepared, counted, and diluted to 1×10^6 cells/100 μ L. Subsequently, cells were stained for DR4 (DJR1-APC,
586 Cat: 307208, Biolegend) and DR5 (DJR2-4-PE, Cat:307406, Biolegend) markers for 30 min at 4 °C. Cells were
587 then washed twice in ice-cold PBS and stained with viability dye (violet fluorescent reactive dye, Cat:L34955,
588 Invitrogen). FACS Buffer (1% FBS, 0.5 mM EDTA in PBS (400 μ L)) was subsequently added. Cells were not
589 fixed or permeabilized. Stained samples were analyzed using single-color compensation and FMO controls on
590 a Sony SP6800 spectral analyzer and quantified using FlowJo V10.8.1 (BD Biosciences). Cells were gated in
591 the following sequence: SSC-A x FSC-A, FSC-H x FSC-A, SSC-H x SSC-A, and Live Cells, to determine Mean
592 Fluorescence Intensity (MFI) of DR5 or DR4.

593

594 Statistical Analysis

595 Statistical analysis of protein levels detected by immunoblot, MTT viability assays and protein synthesis assays
596 were performed as described in a previous publication [33].

597

598

Figure Legends

Fig. 1: DDA compounds that selectively inhibit AGR2, PDIA1, and ERp44 block the maturation of select transmembrane and secreted proteins, but strongly upregulate DR5. A. Chemical structures of representative DDAs used in the manuscript. B. Demonstration of the selectivity of biotinylated DDA binding to the target proteins PDIA1, ERp44, and AGR2. Extracts from T47D cells were incubated with the indicated competitors for 2h and then incubated for 1 h with biotinylated-DDA, followed by sample analysis by gel electrophoresis and blotting with Streptavidin-Alkaline Phosphatase detection. C. Non-reducing immunoblot analysis of the effect of 24 h treatment of the indicated cells with the specified DDAs at 2.5 μ M each. M represents monomeric DR5 isoforms and O represents disulfide-bonded DR5 oligomeric complexes. S and L refer to the short and long forms of DR5 and S' and L' refer to the same DR5 isoforms with altered electrophoretic mobility caused by DDA treatment. Actin serves as a loading control. D. Left panel, reducing immunoblot analysis of MDA-MB-468 cells treated with increasing dFtcyDTDO concentrations showing higher expression of XBP1s and decreased levels of the mature forms and increased relative levels of the pro- forms of MET and PCSK9. Right panel, non-reducing immunoblot analysis using the indicated antibodies. Red arrows represent oligomeric ERp44 isoforms lost upon dFtcyDTDO treatment and the green arrow represents high molecular mass ERp44 isoforms elevated by dFtcyDTDO treatment. O and M represent the Oligomeric and Monomeric protein isoforms in panels C and D.

Fig. 2: PERK inhibition amplifies the pro-apoptotic effects of DDAs on cancer cell lines. A. Reducing immunoblot analysis of MDA-MB-468 cells treated for 24 h with the indicated combinations of dMtcyDTDO (2.5 μ M), Rapamycin (100 nM), TORIN1 (100 nM), MK2206 (5 μ M), Gefitinib (10 μ M), Lapatinib (10 μ M), Thapsigargin (400 nM), and PERKi (1 μ M). Red arrows denote pro- or mature protein isoforms. B. MTT cell viability assays of MDA-MB-468 cells (left panel) or WM793 cells (right panel) treated for 72 h as indicated. Data are plotted as the average (N = 6), with error bars representing standard deviation. C. Reducing immunoblot analysis of HepG2 or MDA-MB-468 cells treated for 24 h as indicated with 2.5 μ M dMtcyDTDO or 1 μ M PERKi. Red arrows denote pro- or mature protein isoforms. D. Reducing immunoblot analysis of the indicated cell lines treated as specified for 24 h with dMtcyDTDO (2.5 μ M) or PERKi (1 μ M). E. Reducing

627 immunoblot analysis of MDA-MB-468 cells or SUM149pt cells treated for 24 h as indicated with dMtcyDTDO
628 (2.5 μ M), ISRIB (200 nM), or PERKi (1 μ M).
629
630 **Fig. 3:** A variety of ER stressors alter DR5 disulfide bonding. A, upper panel. ERp44-deficient HepG2 cells into
631 which vector, wild type or catalytically null ERp44 were reintroduced were treated as indicated for 24 h and
632 analyzed by non-reducing immunoblot. A, lower panel. Expanded region of the DR5 immunoblot showing
633 altered DR5 disulfide bonding in the Thapsigargin/PERKi combination treatment. B. Non-reducing immunoblot
634 of MDA-MB-468 cells treated as indicated for 24 h. C. MDA-MB-468 cells were treated as indicated for 24 h
635 and subjected to non-reducing (DR5, Cleaved Caspase 3, DR4, Actin) or reducing (MET) immunoblot analysis.
636 D. Protein synthesis assays of cells pre-treated for 24 h as indicated before protein synthesis was measured
637 by 3 H-Leucine incorporation over a 2 h pulse. Data are plotted as the average (N = 6), with error bars
638 representing standard deviation. E. HepG2 cells were treated as indicated for 24 h and subjected to non-
639 reducing (DR5, Cleaved Caspase 3, DR4, Actin) or reducing (MET) immunoblot analysis. F. Control and PERK
640 knockout HepG2 cells were treated for 24 h as indicated and subjected to non-reducing immunoblot analysis.
641 G. Non-reducing immunoblot analysis of the indicated cell lines treated as specified for 24 h. Note the DR5
642 oligomerization in A431 cells when Thapsigargin, Tunicamycin, or dFtcyDTDO are combined with PERK
643 inhibition. H. Non-reducing immunoblot analysis of WM793 cells treated as specified for 24 h. Unless otherwise
644 specified, the following concentrations of compounds were used in A-H above: dFtcyDTDO (2.5 μ M),
645 Thapsigargin (400 nM), Tunicamycin (500 ng/ml), Cyclosporine A (10 μ M), Dithiothreitol (DTT; (2.5 mM)),
646 ISRIB (200 nM), or PERKi (1 μ M). O and M represent Oligomeric and Monomeric protein isoforms in panels A,
647 C, E, G, and H.
648

649 **Fig. 4:** DDA upregulation of DR5 occurs in breast cancer cells or mammary epithelial cells overexpressing
650 MYC or EGFR. A. The indicated cell lines were treated for 24 h with 2.5 μ M dMtcyDTDO or dFtcyDTDO and
651 analyzed by immunoblot under reducing conditions. B. MDA-MB-468 cells or Human Mammary Epithelial Cells
652 (HMEC) were treated for 24 h as indicated and subjected to non-reducing immunoblot. D may represent PERK
653 degradation products produced by Caspases. C. MCF10A cells engineered to overexpress EGFR or the

654 corresponding vector control line were treated as indicated for 24 h with 2.5 μ M dFtcyDTDO, 10 μ M
655 Cyclosporine A, or vehicle. The medium was collected and concentrated for analysis of secreted proteins and
656 the cell extracts were analyzed for internal proteins. Immunoblot analysis was performed under non-reducing
657 conditions. O and M represent Oligomeric and Monomeric protein isoforms in panels B and C. D. MCF10A
658 cells engineered to overexpress EGFR or MYC were treated for 24 h with 2.5 μ M dFtcyDTDO or vehicle and
659 cells were analyzed by non-reducing immunoblot. Bands shown represent monomeric protein isoforms.

660

661 **Fig. 5:** Genetic disruption of multiple DR5 disulfide bonds induces its stabilization and pro-apoptotic signaling.
662 A. Structural model of DR5 showing its disulfide bonds, and the positive patch autoinhibitory domain described
663 in the literature. B. Non-reducing immunoblot analysis of MDA-MB-468 cells engineered with doxycycline-
664 inducible expression of wild type (WT) DR5 or the indicated Cys to Ser disulfide bond mutants. Cells were
665 treated as indicated for 24 h with 1 μ g/ml doxycycline and 2.5 μ M dMtcyDTDO. The red arrow denotes DR4
666 oligomers that coincide with DR5 oligomerization. C. Reducing immunoblot analysis of the indicated MDA-MB-
667 468 stable cell lines. Cells were treated for 24 h as specified with 1 μ g/ml doxycycline or doxycycline + 10 μ M
668 Q-VD-OPH. The catalog numbers of DR5 and DR4 antibodies are shown. D. Non-reducing immunoblot
669 analysis of the indicated MDA-MB-468 cell lines with doxycycline-inducible expression of wild type DR4 and
670 DR5, and DR4 and DR5 C-terminal deletion constructs defective in apoptotic signaling. Cells were treated for
671 24 h as specified with 1 μ g/ml doxycycline or doxycycline + 2.5 μ M dMtcyDTDO. E. Non-reducing immunoblot
672 analysis of the indicated MDA-MB-468 cell lines with doxycycline-inducible expression of wild type and
673 apoptosis-defective DR5. Cells were treated for 24 h as specified with 1 μ g/ml doxycycline or doxycycline + 2.5
674 μ M dMtcyDTDO. F. Non-reducing immunoblot analysis of the indicated MDA-MB-468 doxycycline-inducible
675 stable cell lines. Cells were treated for 24 h as indicated. G. Non-reducing immunoblot analysis of the indicated
676 MDA-MB-468 cell lines with doxycycline-inducible expression of wild type and apoptosis-defective DR5. Cells
677 were treated for 24 h as specified with 1 μ g/ml doxycycline or doxycycline + 2.5 μ M dMtcyDTDO. O and M
678 represent Oligomeric and Monomeric protein isoforms in panels B and D-G.

679

680 **Fig. 6:** DDAs activate autophagy and inhibitors of autophagy/lysosomal degradation upregulate DR5. A. Non-
681 reducing immunoblot analysis of MDA-MB-468 cells treated as indicated for 24 h. B. Non-reducing immunoblot
682 analysis of vector control or DR5 knockout MDA-MB-468 cells treated with 2.5 μ M dFtcyDTDO or 1 μ M
683 Bafilomycin A1 for 24 h. C. Non-reducing immunoblot analysis of MDA-MB-468 cells treated for 24 h as
684 indicated with 1 μ M PERKi (P), 15 μ M Chloroquine (C), or 2.5 μ M dFtcyDTDO (dF). D. MTT Cell viability assay
685 of MDA-MB-468 cells treated as indicated for 72 h. Data are plotted as the average (N = 6), with error bars
686 representing standard deviation. E. Non-reducing immunoblot analysis of MDA-MB-468 cells treated for 24 h
687 as indicated with 2.5 μ M dFtcyDTDO (F) or 1 μ M Bafilomycin A1 (BFA1), VPS34 inhibitor (VPS34i), 400 nM
688 Thapsigargin, or 500 ng/ml Tunicamycin. O and M represent Oligomeric and Monomeric protein isoforms in
689 panels A, B, C, and E.

690
691 **Fig. 7:** DDAs upregulate TRAIL Decoy Receptor 2, an effect overridden by Cyclosporine A. A. Sequence
692 alignment of the putative autoinhibitory motifs of DR4, DR5, DCR1, and DCR2. B. Non-reducing immunoblot
693 analysis of MDA-MB-468 cells treated for 24 h with the indicated concentrations of dFtcyDTDO, combined with
694 DMSO vehicle, 5 μ M Cyclosporine A or 100 nM FK506. C. Non-reducing immunoblot analysis of MDA-MB-468
695 cells treated for 24 h with the indicated concentrations of dFtcyDTDO, combined with DMSO vehicle or 5 μ M
696 Cyclosporine A. D. Non-reducing immunoblot analysis of MDA-MB-468 cells treated for 24 h with the indicated
697 concentrations of dFtcyDTDO, combined with DMSO vehicle or 5 μ M Cyclosporine A. Data are plotted as the
698 average (N = 3), with error bars representing standard error. Asterisks denote $p < 0.05$ compared to control
699 using Student's unpaired *t*-test. E. Densitometry analysis of the relative levels of total, monomeric, and
700 oligomeric forms of DR5 (left panel) or total levels of Cyclophilin B or DCR2 (right panel) from panels 7B-D. O
701 and M represent Oligomeric and Monomeric protein isoforms in panels B-D.

702
703 **Fig. 8:** Effects of altered disulfide bonding on DR5 cell surface localization and antibody recognition. A. Flow
704 cytometry analysis of the indicated doxycycline-inducible MDA-MB-468 stable cell lines with an antibody to
705 DR5 (Clone DJR2-4 (7-8)) (top panel) or DR4 (bottom panel). Prior to analysis, cells were treated for 24 h as
706 indicated with 10 μ M Q-VD-OPH, 1 μ g/ml doxycycline, or 2.5 μ M dFtcyDTDO. Dots represent the average

707 values from three independent biological replicates performed in triplicate. * Represents $p < 0.05$, ****
708 represents $p < 0.0001$, and ns represents not significant ($p > 0.05$). B. Non-reducing immunoblot analysis of
709 the indicated MDA-MB-468 stable cell lines treated for 24 h as specified. Note the alternate staining patterns
710 observed with different DR5 antibodies. O and M represent Oligomeric and Monomeric protein isoforms. C.
711 The indicated MDA-MB-468 stable cell lines were treated for 24 h as indicated with 1 $\mu\text{g/ml}$ doxycycline and
712 2.5 μM dFtcyDTDO and subjected to cell surface protein biotin labeling. Cell surface proteins (External; Ext.)
713 were affinity purified with Streptavidin-agarose, and the unlabeled flow-through (Internal; Int.) proteins were
714 also collected. Both fractions were analyzed by non-reducing immunoblot using the indicated antibodies. D.
715 Cell surface protein labeling experiment as in panel C except that cell lines were treated with the indicated
716 combinations of 1 $\mu\text{g/ml}$ doxycycline, 2.5 μM dFtcyDTDO, and 10 μM Cyclosporine A.

717

718 **Fig. 9:** Metabolic stability of select DDAs and lack of DDA effects on liver morphology. A. Hematoxylin and
719 Eosin stained breast tumor (upper panels) and liver tissue samples (lower panels) from mice bearing
720 012/LVM2/LR10 tumors after treatment with vehicle (peanut oil) or 10 mg/kg dMtcyDTDO by oral gavage for 20
721 days. B. Stability of tcyDTDO, dMtcyDTDO, or dFtcyDTDO metabolism in rat or human liver microsomes in the
722 presence or absence of 1 mM NADPH. Verapamil serves as a positive control. C. Stability of tcyDTDO,
723 dMtcyDTDO metabolism, or dFtcyDTDO in rat or human intestinal microsomes in the presence or absence of 1
724 mM NADPH. Verapamil serves as a positive control. Data points are plotted as the average ($N = 3$), with error
725 bars representing standard deviation.

726

727 **References**

- 728
729 1 Ye ZW, Zhang J, Aslam M, Blumental-Perry A, Tew KD, Townsend DM. Protein disulfide isomerase
730 family mediated redox regulation in cancer. *Adv Cancer Res* 2023; 160: 83-106.
- 731
732 2 Zelencova-Gopejenko D, Andrianov V, Domracheva I, Kanepe-Lapsa I, Milczarek M, Stojak M *et al.*
733 Aromatic sulphonamides of aziridine-2-carboxylic acid derivatives as novel PDIA1 and PDIA3 inhibitors.
734 *J Enzyme Inhib Med Chem* 2023; 38: 2158187.
- 735
736 3 Mouawad R, Neamati N. Inhibition of Protein Disulfide Isomerase (PDIA1) Leads to Proteasome-
737 Mediated Degradation of Ubiquitin-like PHD and RING Finger Domain-Containing Protein 1 (UHRF1)
738 and Increased Sensitivity of Glioblastoma Cells to Topoisomerase II Inhibitors. *ACS Pharmacol Transl*
739 *Sci* 2023; 6: 100-114.
- 740
741 4 Germon A, Heesom KJ, Amoah R, Adams JC. Protein disulfide isomerase A3 activity promotes
742 extracellular accumulation of proteins relevant to basal breast cancer outcomes in human MDA-MB-
743 A231 breast cancer cells. *Am J Physiol Cell Physiol* 2023; 324: C113-C132.
- 744
745 5 Chichiarelli S, Altieri F, Paglia G, Rubini E, Minacori M, Eufemi M. ERp57/PDIA3: new insight. *Cell Mol*
746 *Biol Lett* 2022; 27: 12.
- 747
748 6 Edupuganti R, Wang Q, Tavares CD, Chitjian CA, Bachman JL, Ren P *et al.* Synthesis and biological
749 evaluation of pyrido[2,3-d]pyrimidine-2,4-dione derivatives as eEF-2K inhibitors. *Bioorg Med Chem*
750 2014; 22: 4910-4916.
- 751
752 7 Law ME, Yaaghubi E, Ghilardi AF, Davis BJ, Ferreira RB, Koh J *et al.* Inhibitors of ERp44, PDIA1, and
753 AGR2 induce disulfide-mediated oligomerization of Death Receptors 4 and 5 and cancer cell death.
754 *Cancer Lett* 2022; 534: 215604.
- 755
756 8 Wang M, Law ME, Davis BJ, Yaaghubi E, Ghilardi AF, Ferreira RB *et al.* Disulfide bond-disrupting
757 agents activate the tumor necrosis family-related apoptosis-inducing ligand/death receptor 5 pathway.
758 *Cell Death Discov* 2019; 5: 153.
- 759
760 9 Wang M, Ferreira RB, Law ME, Davis BJ, Yaaghubi E, Ghilardi AF *et al.* A novel proteotoxic
761 combination therapy for EGFR+ and HER2+ cancers. *Oncogene* 2019; 38: 4264-4282.
- 762
763 10 Ghilardi AF, Yaaghubi E, Ferreira RB, Law ME, Yang Y, Davis BJ *et al.* Anticancer Agents Derived from
764 Cyclic Thiosulfonates: Structure-Reactivity and Structure-Activity Relationships. *ChemMedChem* 2022;
765 17: e202200165.
- 766
767 11 D'Arcy P, Brnjic S, Olofsson MH, Fryknas M, Lindsten K, De Cesare M *et al.* Inhibition of proteasome
768 deubiquitinating activity as a new cancer therapy. *Nat Med* 2011; 17: 1636-1640.
- 769
770 12 Mahameed M, Boukeileh S, Obiedat A, Darawshi O, Dipta P, Rimon A *et al.* Pharmacological induction
771 of selective endoplasmic reticulum retention as a strategy for cancer therapy. *Nat Commun* 2020; 11:
772 1304.

- 773
774 13 Sidrauski C, Acosta-Alvear D, Khoutorsky A, Vedantham P, Hearn BR, Li H *et al.* Pharmacological
775 brake-release of mRNA translation enhances cognitive memory. *Elife* 2013; 2: e00498.
- 776
777 14 Harding HP, Zhang Y, Zeng H, Novoa I, Lu PD, Calton M *et al.* An integrated stress response regulates
778 amino acid metabolism and resistance to oxidative stress. *Molecular cell* 2003; 11: 619-633.
- 779
780 15 Law ME, Ferreira RB, Davis BJ, Higgins PJ, Kim JS, Castellano RK *et al.* CUB domain-containing
781 protein 1 and the epidermal growth factor receptor cooperate to induce cell detachment. *Breast Cancer*
782 *Res* 2016; 18: 80.
- 783
784 16 Ferreira RB, Law ME, Jahn SC, Davis BJ, Heldermon CD, Reinhard M *et al.* Novel agents that
785 downregulate EGFR, HER2, and HER3 in parallel. *Oncotarget* 2015; 6: 10445-10459.
- 786
787 17 Ferreira RB, Wang M, Law ME, Davis BJ, Bartley AN, Higgins PJ *et al.* Disulfide bond disrupting agents
788 activate the unfolded protein response in EGFR- and HER2-positive breast tumor cells. *Oncotarget*
789 2017; 8: 28971-28989.
- 790
791 18 Armstrong DK, Kaufmann SH, Ottaviano YL, Furuya Y, Buckley JA, Isaacs JT, Davidson NE. Epidermal
792 growth factor-mediated apoptosis of MDA-MB-468 human breast cancer cells. *Cancer Res* 1994; 54:
793 5280-5283.
- 794
795 19 Vitello EA, Quek SI, Kincaid H, Fuchs T, Crichton DJ, Troisch P, Liu AY. Cancer-secreted AGR2
796 induces programmed cell death in normal cells. *Oncotarget* 2016; 7: 49425-49434.
- 797
798 20 Ho ME, Quek SI, True LD, Seiler R, Fleischmann A, Bagryanova L *et al.* Bladder cancer cells secrete
799 while normal bladder cells express but do not secrete AGR2. *Oncotarget* 2016; 7: 15747-15756.
- 800
801 21 Clarke C, Rudland P, Barraclough R. The metastasis-inducing protein AGR2 is O-glycosylated upon
802 secretion from mammary epithelial cells. *Mol Cell Biochem* 2015; 408: 245-252.
- 803
804 22 Bergstrom JH, Berg KA, Rodriguez-Pineiro AM, Stecher B, Johansson ME, Hansson GC. AGR2, an
805 endoplasmic reticulum protein, is secreted into the gastrointestinal mucus. *PLoS One* 2014; 9:
806 e104186.
- 807
808 23 Stocki P, Chapman DC, Beach LA, Williams DB. Depletion of cyclophilins B and C leads to
809 dysregulation of endoplasmic reticulum redox homeostasis. *J Biol Chem* 2014; 289: 23086-23096.
- 810
811 24 Pan L, Fu TM, Zhao W, Zhao L, Chen W, Qiu C *et al.* Higher-Order Clustering of the Transmembrane
812 Anchor of DR5 Drives Signaling. *Cell* 2019; 176: 1477-1489 e1414.
- 813
814 25 Shivange G, Mondal T, Lyerly E, Bhatnagar S, Landen CN, Reddy S *et al.* A patch of positively charged
815 residues regulates the efficacy of clinical DR5 antibodies in solid tumors. *Cell Rep* 2021; 37: 109953.
- 816

- 817 26 Mongkolsapaya J, Grimes JM, Chen N, Xu X-N, Stuart DI, Jones EY, Screaton GR. Structure of the
818 TRAIL–DR5 complex reveals mechanisms conferring specificity in apoptotic initiation. *Nature Structural*
819 *Biology* 1999; 6: 1048-1053.
- 820
821 27 Caserta TM, Smith AN, Gultice AD, Reedy MA, Brown TL. Q-VD-OPh, a broad spectrum caspase
822 inhibitor with potent antiapoptotic properties. *Apoptosis* 2003; 8: 345-352.
- 823
824 28 Ferreira KS, Kreutz C, Macnelly S, Neubert K, Haber A, Bogyo M *et al.* Caspase-3 feeds back on
825 caspase-8, Bid and XIAP in type I Fas signaling in primary mouse hepatocytes. *Apoptosis* 2012; 17:
826 503-515.
- 827
828 29 Thomas LR, Johnson RL, Reed JC, Thorburn A. The C-terminal tails of tumor necrosis factor-related
829 apoptosis-inducing ligand (TRAIL) and Fas receptors have opposing functions in Fas-associated death
830 domain (FADD) recruitment and can regulate agonist-specific mechanisms of receptor activation. *J Biol*
831 *Chem* 2004; 279: 52479-52486.
- 832
833 30 Castino R, Davies J, Beaucourt S, Isidoro C, Murphy D. Autophagy is a prosurvival mechanism in cells
834 expressing an autosomal dominant familial neurohypophyseal diabetes insipidus mutant vasopressin
835 transgene. *FASEB J* 2005; 19: 1021-1023.
- 836
837 31 Limpert AS, Lambert LJ, Bakas NA, Bata N, Brun SN, Shaw RJ, Cosford NDP. Autophagy in Cancer:
838 Regulation by Small Molecules. *Trends Pharmacol Sci* 2018; 39: 1021-1032.
- 839
840 32 Lam M, Marsters SA, Ashkenazi A, Walter P. Misfolded proteins bind and activate death receptor 5 to
841 trigger apoptosis during unresolved endoplasmic reticulum stress. *Elife* 2020; 9.
- 842
843 33 Law ME, Davis BJ, Ghilardi AF, Yaaghubi E, Dulloo ZM, Wang M *et al.* Repurposing Tranexamic Acid
844 as an Anticancer Agent. *Frontiers in Pharmacology (Original Research)* 2022; 12.
- 845
846 34 Law ME, Yaaghubi E, Ghilardi AF, Davis BJ, Ferreira RB, Koh J *et al.* Inhibitors of ERp44, PDIA1, and
847 AGR2 induce disulfide-mediated oligomerization of Death Receptors 4 and 5 and cancer cell death.
848 *bioRxiv* 2021: 2021.2001.2013.426390.
- 849
850 35 Yamaguchi H, Wang HG. CHOP is involved in endoplasmic reticulum stress-induced apoptosis by
851 enhancing DR5 expression in human carcinoma cells. *J Biol Chem* 2004; 279: 45495-45502.
- 852
853 36 Chen G, Fan Z, Wang X, Ma C, Bower KA, Shi X *et al.* Brain-derived neurotrophic factor suppresses
854 tunicamycin-induced upregulation of CHOP in neurons. *J Neurosci Res* 2007; 85: 1674-1684.
- 855
856 37 Calvo V, Zheng W, Adam-Artigues A, Staschke KA, Huang X, Cheung JF *et al.* A PERK-Specific
857 Inhibitor Blocks Metastatic Progression by Limiting Integrated Stress Response-Dependent Survival of
858 Quiescent Cancer Cells. *Clin Cancer Res* 2023; 29: 5155-5172.
- 859
860 38 Zhang B, van Roosmalen IAM, Reis CR, Setroikromo R, Quax WJ. Death receptor 5 is activated by
861 fucosylation in colon cancer cells. *FEBS J* 2019; 286: 555-571.
- 862

- 863 39 Micheau O. Regulation of TNF-Related Apoptosis-Inducing Ligand Signaling by Glycosylation. *Int J Mol*
864 *Sci* 2018; 19.
- 865
866 40 Yoshida T, Shiraishi T, Horinaka M, Wakada M, Sakai T. Glycosylation modulates TRAIL-R1/death
867 receptor 4 protein: different regulations of two pro-apoptotic receptors for TRAIL by tunicamycin. *Oncol*
868 *Rep* 2007; 18: 1239-1242.
- 869
870 41 Wagner KW, Punnoose EA, Januario T, Lawrence DA, Pitti RM, Lancaster K *et al.* Death-receptor O-
871 glycosylation controls tumor-cell sensitivity to the proapoptotic ligand Apo2L/TRAIL. *Nat Med* 2007; 13:
872 1070-1077.
- 873
874 42 Huang L, Che Z, Liu F, Ge M, Wu Z, Wu L *et al.* ASB3 promotes hepatocellular carcinoma progression
875 by mediating DR5 ubiquitination in TRAIL resistance. *FASEB J* 2024; 38: e23475.
- 876
877 43 Zhang S, Chen Z, Shi P, Fan S, He Y, Wang Q *et al.* Downregulation of death receptor 4 is tightly
878 associated with positive response of EGFR mutant lung cancer to EGFR-targeted therapy and
879 improved prognosis. *Theranostics* 2021; 11: 3964-3980.
- 880
881 44 Wang Q, Chen Q, Zhu L, Chen M, Xu W, Panday S *et al.* JWA regulates TRAIL-induced apoptosis via
882 MARCH8-mediated DR4 ubiquitination in cisplatin-resistant gastric cancer cells. *Oncogenesis* 2017; 6:
883 e353.
- 884
885 45 Iwawaki T, Hosoda A, Okuda T, Kamigori Y, Nomura-Furuwatari C, Kimata Y *et al.* Translational control
886 by the ER transmembrane kinase/ribonuclease IRE1 under ER stress. *Nat Cell Biol* 2001; 3: 158-164.
- 887
888 46 Neidhardt L, Cloots E, Friemel N, Weiss CAM, Harding HP, McLaughlin SH *et al.* The IRE1beta-
889 mediated unfolded protein response is repressed by the chaperone AGR2 in mucin producing cells.
890 *EMBO J* 2023.
- 891
892 47 Cloots E, Guilbert P, Provost M, Neidhardt L, Van de Velde E, Fayazpour F *et al.* Activation of goblet-
893 cell stress sensor IRE1 β is controlled by the mucin chaperone AGR2. *The EMBO Journal* 2023: 1-24-
894 24.
- 895
896 48 Kato T, Lim B, Cheng Y, Pham A-T, Maynard J, Moreau D *et al.* Cyclic Thiosulfonates for Thiol-
897 Mediated Uptake: Cascade Exchangers, Transporters, Inhibitors. *JACS Au* 2022; 2: 839-852.
- 898
899 49 Zeisel L, Felber JG, Scholzen KC, Schmitt C, Wiegand AJ, Komissarov L *et al.* Piperazine-Fused Cyclic
900 Disulfides Unlock High-Performance Bioreductive Probes of Thioredoxins and Bifunctional Reagents for
901 Thiol Redox Biology. *J Am Chem Soc* 2024.
- 902
903 50 Giannone C, Chelazzi MR, Orsi A, Anelli T, Nguyen T, Buchner J, Sitia R. Biogenesis of secretory
904 immunoglobulin M requires intermediate non-native disulfide bonds and engagement of the protein
905 disulfide isomerase ERp44. *Embo j* 2022; 41: e108518.
- 906
907 51 Tempio T, Orsi A, Sicari D, Valetti C, Yoboue ED, Anelli T, Sitia R. A virtuous cycle operated by ERp44
908 and ERGIC-53 guarantees proteostasis in the early secretory compartment. *iScience* 2021; 24:
909 102244.

- 910
911 52 Sannino S, Anelli T, Cortini M, Masui S, Degano M, Fagioli C *et al.* Progressive quality control of
912 secretory proteins in the early secretory compartment by ERp44. *J Cell Sci* 2014; 127: 4260-4269.
- 913
914 53 Cortini M, Sitia R. ERp44 and ERGIC-53 synergize in coupling efficiency and fidelity of IgM
915 polymerization and secretion. *Traffic* 2010; 11: 651-659.
- 916
917 54 Fraldi A, Zito E, Annunziata F, Lombardi A, Cozzolino M, Monti M *et al.* Multistep, sequential control of
918 the trafficking and function of the multiple sulfatase deficiency gene product, SUMF1 by PDI, ERGIC-53
919 and ERp44. *Hum Mol Genet* 2008; 17: 2610-2621.
- 920
921 55 Anelli T, Ceppi S, Bergamelli L, Cortini M, Masciarelli S, Valetti C, Sitia R. Sequential steps and
922 checkpoints in the early exocytic compartment during secretory IgM biogenesis. *EMBO J* 2007; 26:
923 4177-4188.
- 924
925 56 Jahn SC, Corsino PE, Davis BJ, Law ME, Norgaard P, Law BK. Constitutive Cdk2 activity promotes
926 aneuploidy while altering the spindle assembly and tetraploidy checkpoints. *J Cell Sci* 2013; 126: 1207-
927 1217.
- 928
929 57 Law BK, Chytil A, Dumont N, Hamilton EG, Waltner-Law ME, Aakre ME *et al.* Rapamycin potentiates
930 transforming growth factor beta-induced growth arrest in nontransformed, oncogene-transformed, and
931 human cancer cells. *Mol Cell Biol* 2002; 22: 8184-8198.
- 932
933 58 Law ME, Davis BJ, Ghilardi AF, Yaaghubi E, Dulloo ZM, Wang M *et al.* Repurposing Tranexamic Acid
934 as an Anticancer Agent. *Front Pharmacol* 2021; 12: 792600.
- 935
936 59 Srivastava PK, Field L. Organic Disulfides and Related Substances .45. Synthesis and Properties of
937 Some Disulfide Sulfinate Salts Containing No Nitrogen. *J Chem Eng Data* 1986; 31: 252-254.
- 938
939 60 Macke JD, Field L. Sulfinic Acids and Related-Compounds .19. Synthesis and Properties of 1-
940 Propanesulfinates, 1-Butanesulfinates, and 1-Pentanesulfinates Terminally Substituted with Disulfide
941 and Trisulfide Functions. *J Org Chem* 1988; 53: 396-402.
- 942
943 61 Ghilardi AF, Yaaghubi E, Ferreira RB, Law ME, Yang Y, Davis BJ *et al.* Anticancer Agents Derived from
944 Cyclic Thiosulfonates: Structure-Reactivity and Structure-Activity Relationships. *ChemMedChem* n/a.
- 945
946 62 Mahmood I. Application of allometric principles for the prediction of pharmacokinetics in human and
947 veterinary drug development. *Adv Drug Deliv Rev* 2007; 59: 1177-1192.
- 948
949 63 Peters SA. *Physiologically based pharmacokinetic (PBPK) modeling and simulations : principles,*
950 *methods, and applications in the pharmaceutical industry.* Wiley: Hoboken, N.J., 2011.
- 951
952 64 Davies B, Morris T. Physiological parameters in laboratory animals and humans. *Pharm Res* 1993; 10:
953 1093-1095.
- 954
955

956 **Acknowledgements**

957 This work was funded in part by the following grants to BL and RC: NIH/NCI R21 CA252400, NIH/NCI R21
958 CA277485, Florida Department of Health, James & Esther King Cancer Research Program grants 23K06 and
959 22K04, Florida Department of Health, Bankhead-Coley Research Program grant 23B03, and a grant from the
960 Florida Breast Cancer Foundation. OG was funded by R01 DK121831. We thank the UF Molecular pathology
961 Core, UF ICBR Proteomics Core, UF CTSI Translational Drug Development Core, and UFHCC Flow
962 Cytometry Core for their contributions to the manuscript.

963

964 **Author Contributions**

965 Performed experiments: MS, ZD, SE, GT, GA, MW, HS, BF, SK, BL

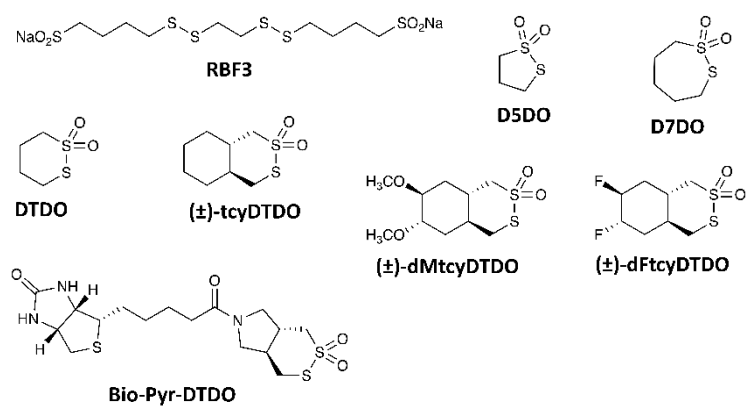
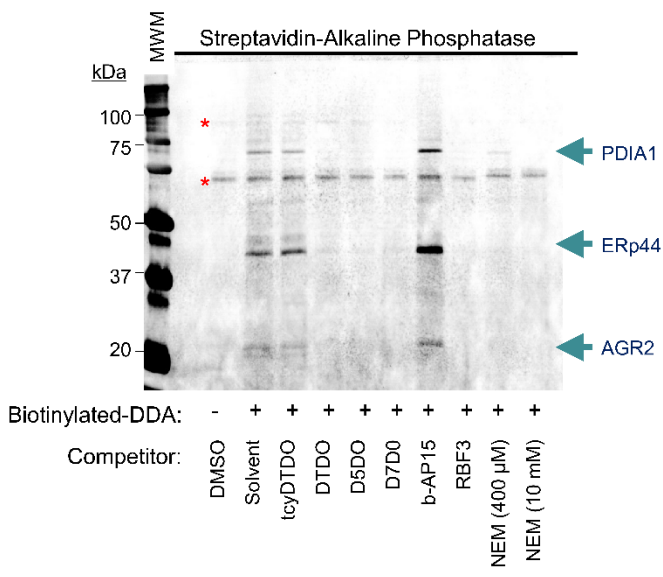
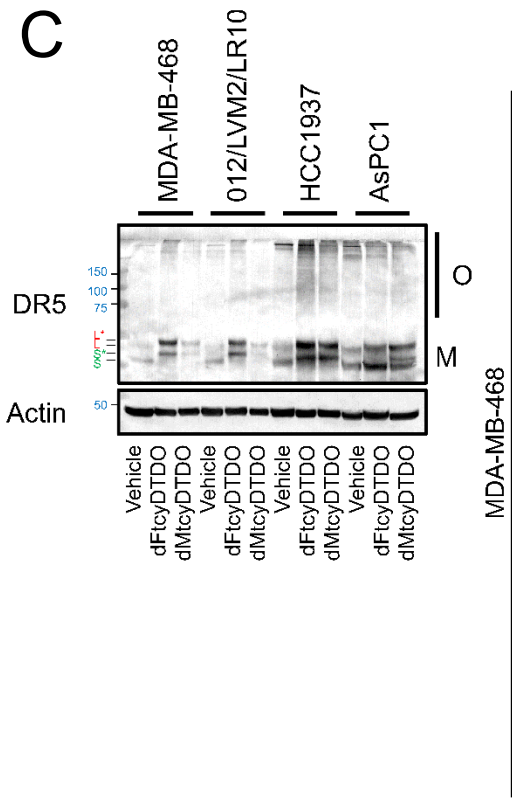
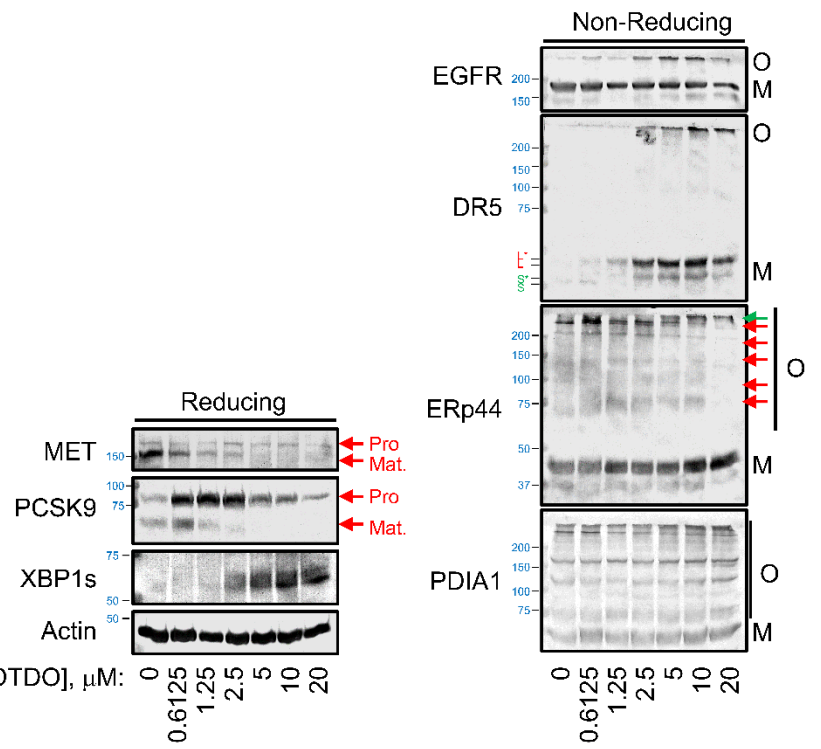
966 Directed research: ML, AS, OG, JH, BT, RC, BL

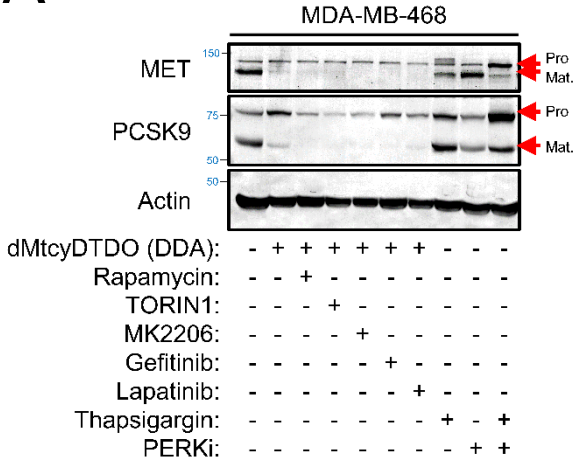
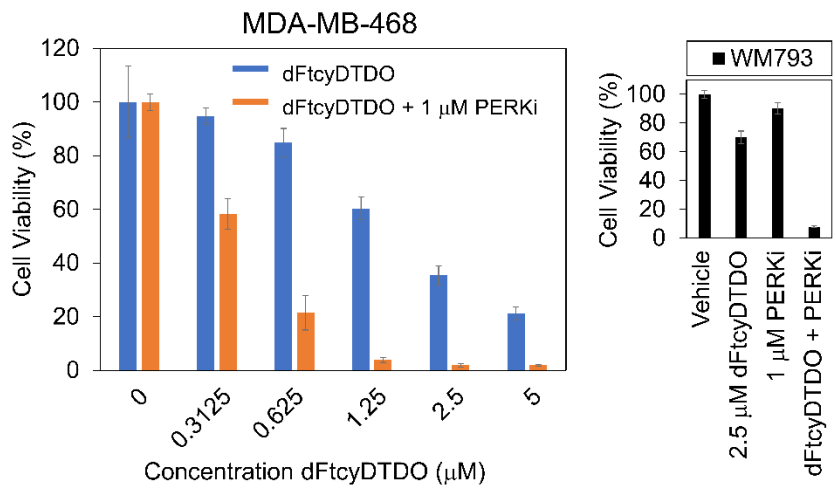
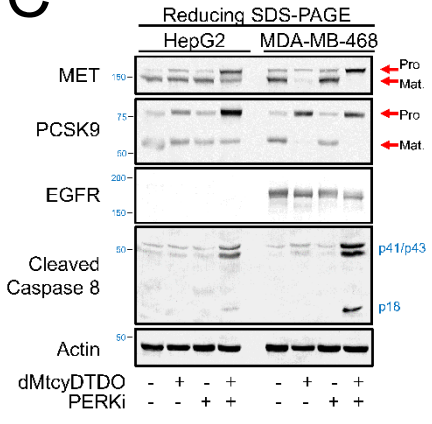
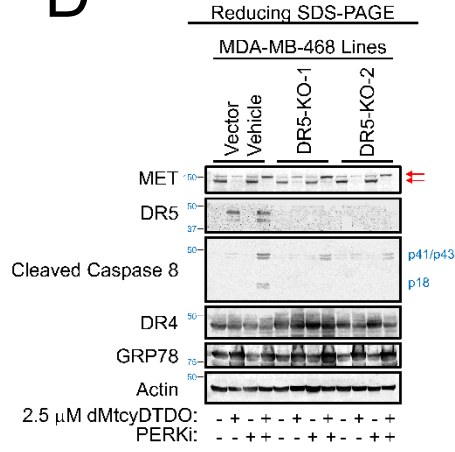
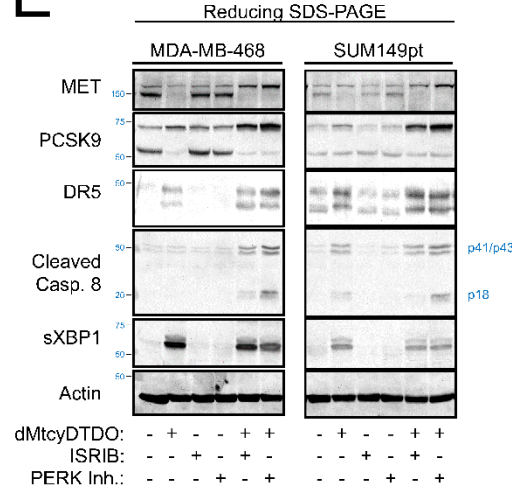
967 Provided key reagents and expertise: JH, BT

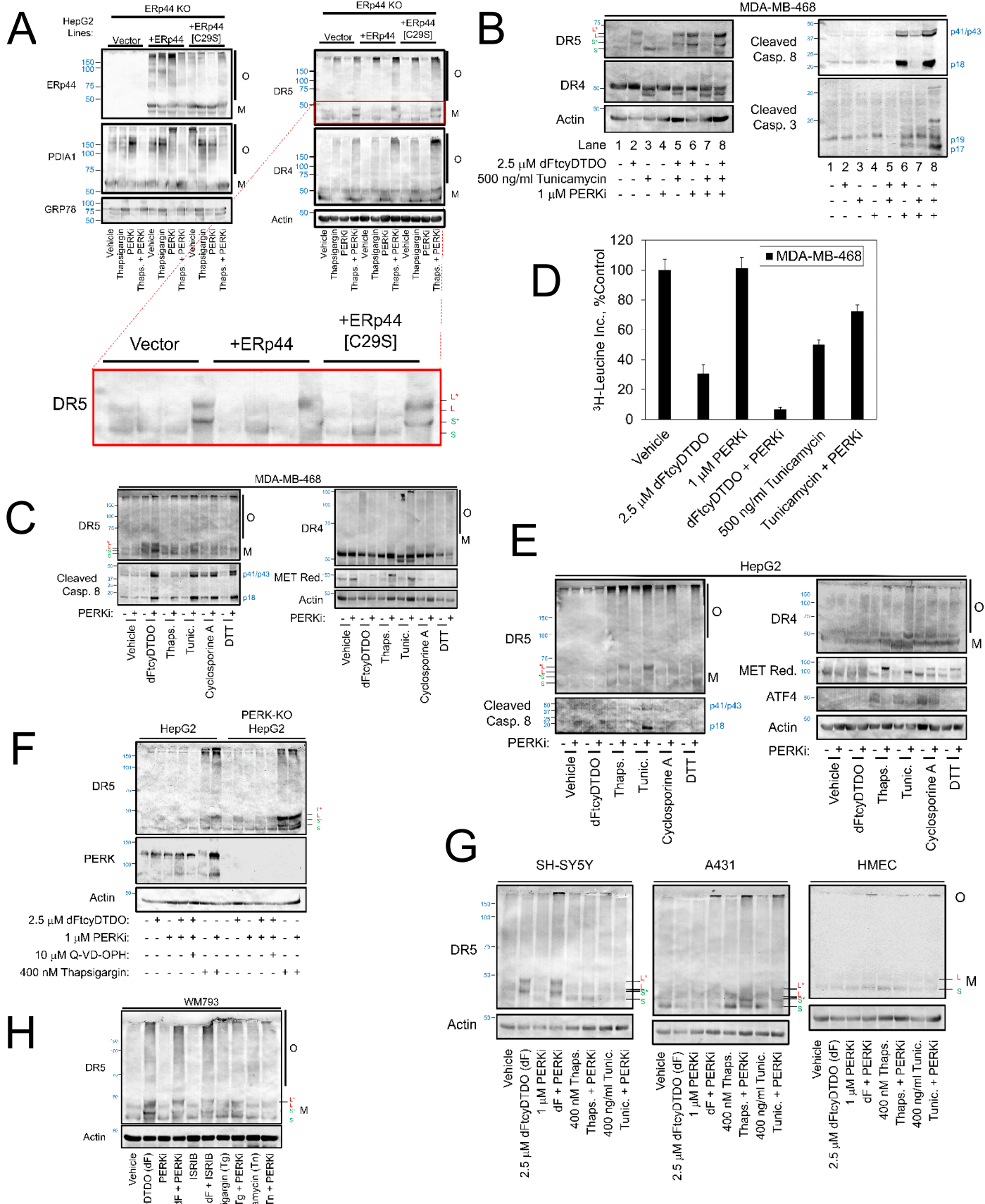
968 Wrote and edited manuscript: ML, ZD, GT, CWC, AS, OG, RC, BL

969

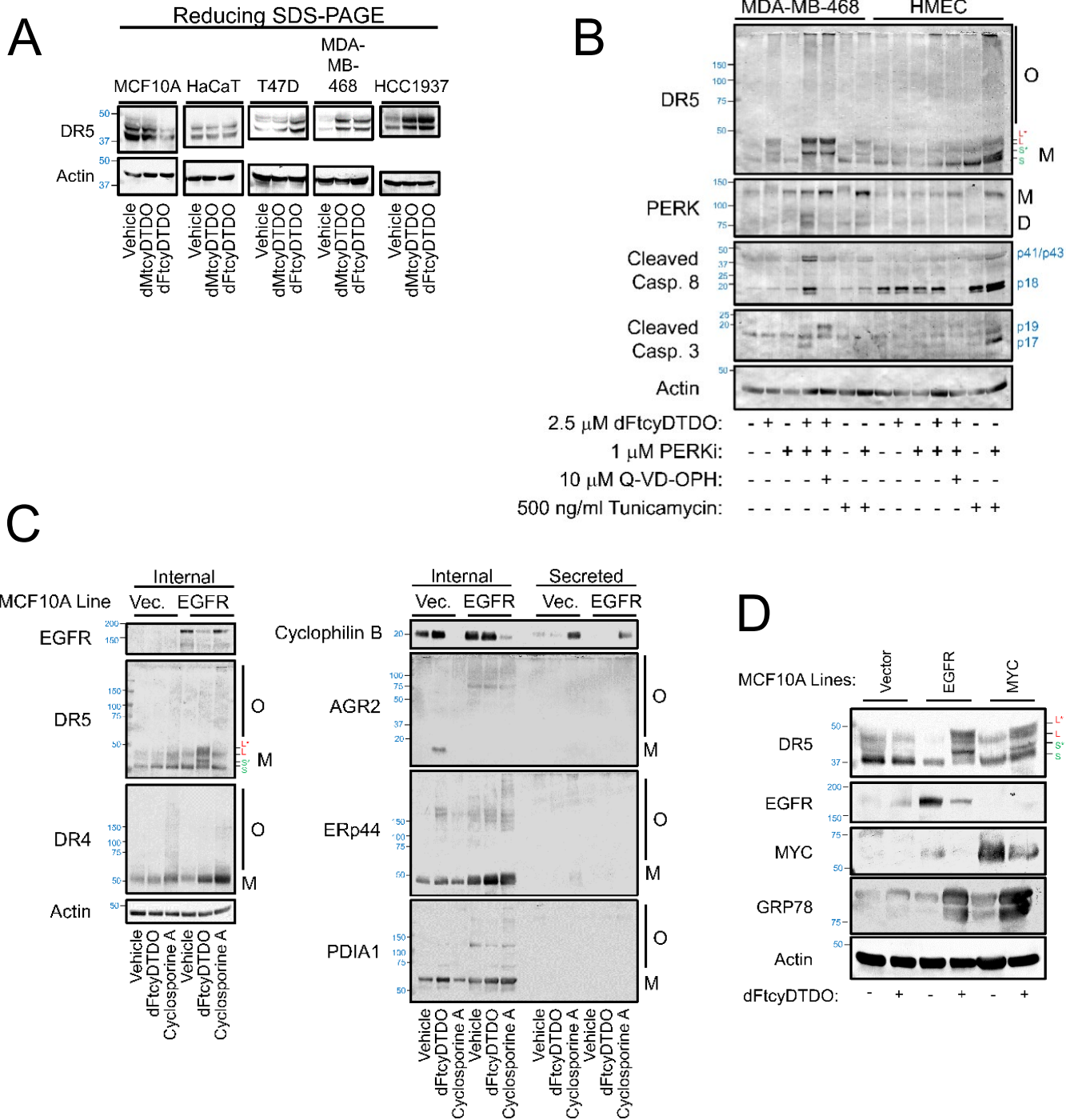
970

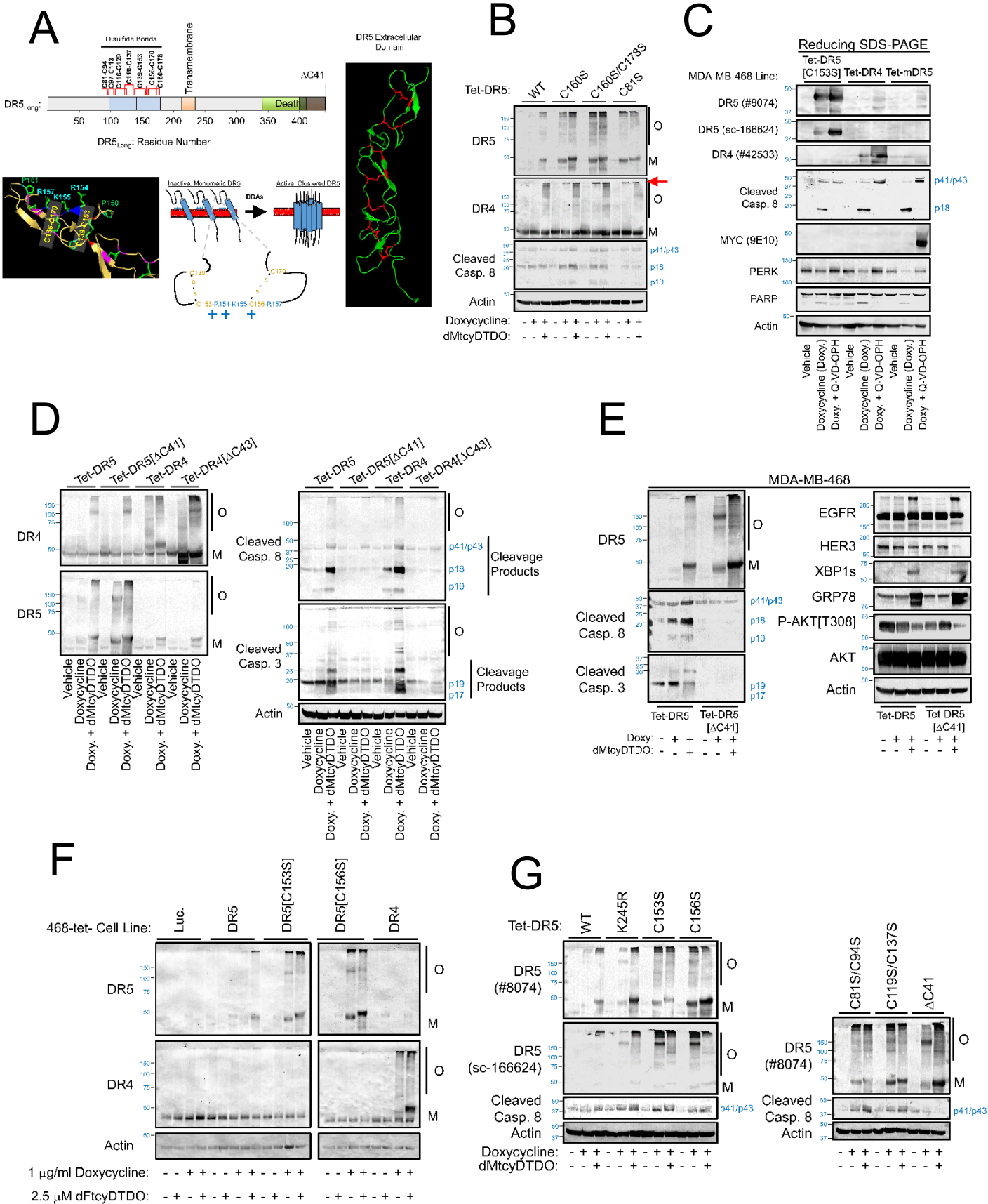
A**B****C****D**

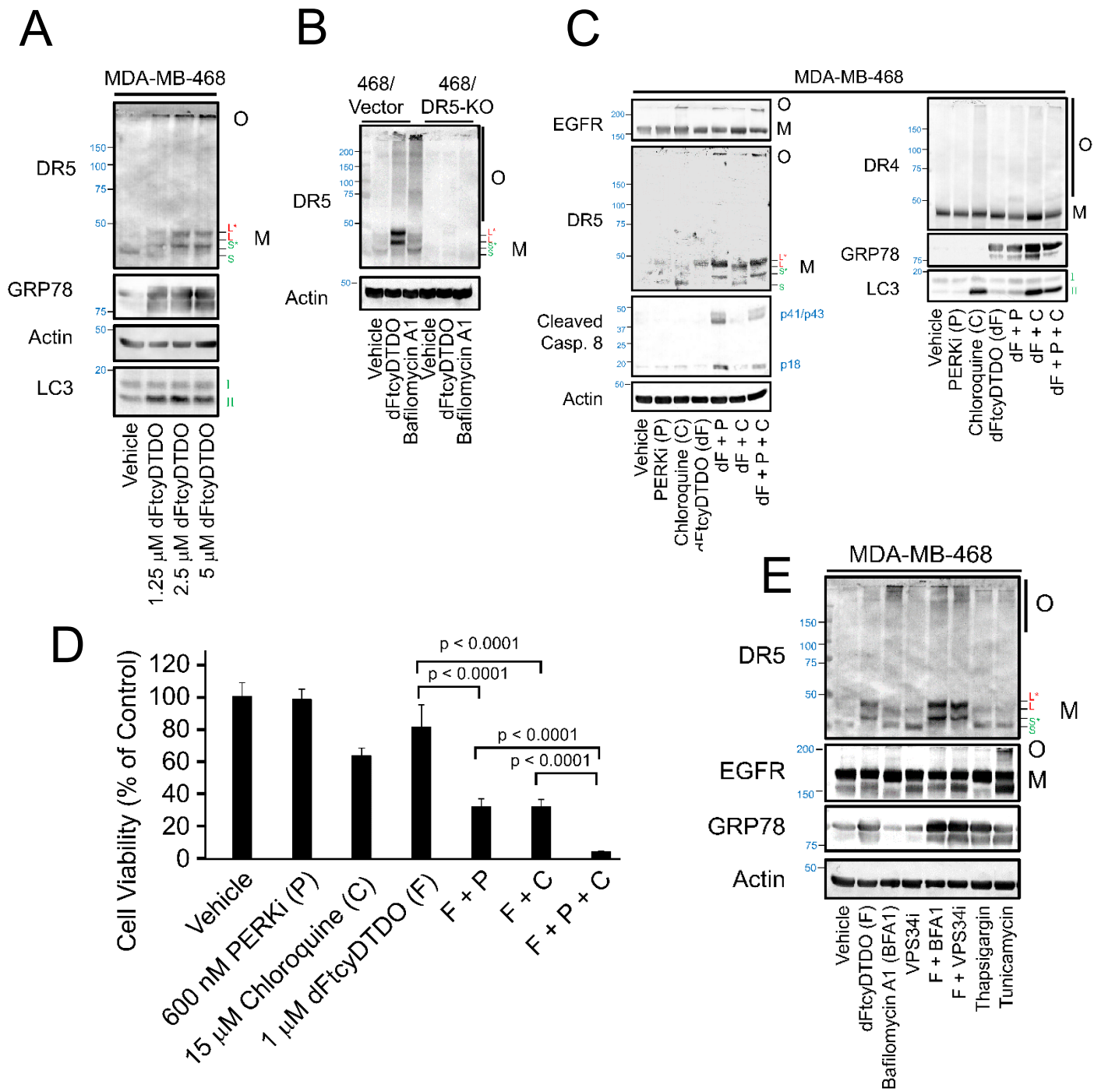
A**B****C****D****E**



Law et al., Fig. 3







Law et al., Fig. 6

A

Protein	Gene	Sequence
DCR1	TR10C_Human	121 SP ^S EM ^E CR ^R CK ^K CS ^S -R ^R CP ^P 132
DCR2	TR10D_Human	151 SP ^S EM ^E CR ^R T ^T CR ^R TG ^G CP ^P 163
DR4	TR10A_Human	200 SA ^S EM ^E CR ^R CK ^K SR ^R GC ^C P ^P 212
DR5	TR10B_Human	149 SP ^S EM ^E CR ^R CK ^K RT ^T GC ^C P ^P 161

* * * * * * * *

